Morphological and functional changes of the blood–brain barrier in hypertriglyceridemia

Ph.D. Thesis

Beáta Barabási

Supervisors:

Mária Deli, M.D., Ph.D, D.Sc

Zsófia Hoyk, Ph.D

Biological Barriers Research Group

Institute of Biophysics, HUN-REN Biological Research Centre, Szeged

Doctoral School of Theoretical Medicine, Albert Szent-Györgyi Medical School

University of Szeged

Szeged, Hungary

2024

TABLE OF CONTENTS

LIST OF PUBLICATIONS 3
LIST OF ABBREVIATIONS 4
1. Introduction 5
2. Aim of the study 10
3. Materials and Methods 11
3.1. Materials 11
3.2. Animals 11
3.3. *In vivo* studies 11
3.3.1. Serum triglyceride measurement 11
3.3.2. *In vivo* permeability measurement of the BBB 12
3.3.3. Immunohistochemistry and confocal microscopy 12
3.4. *In vitro* studies 13
3.4.1. Brain endothelial cell cultures 13
3.4.2. Mixed glial cell cultures 14
3.4.3. Endothelial cell viability assays 15
3.4.4. Cytokine treatments 15
3.4.5. BBB functional assays 15
3.4.5.1. Permeability measurements on BBB co-culture model 15
3.4.5.2. Transendothelial electric resistance on BBB co-culture model 15
3.4.5.3. P-glycoprotein activity on BBB monoculture model 16
3.4.6. Immunocytochemistry and confocal microscopy 16
3.5. *Ex vivo* studies 17
3.5.1. Brain microvessel isolation 17
3.5.2. RNA isolation and quantitative real time PCR 18
3.5.3. Immunohistochemistry on isolated brain microvessels and confocal microscopy 19
3.6. Image analysis 20
3.7. Statistical analysis 20
4. Results 21
4.1. Chronic hypertriglyceridemia in APOB-100 transgenic mice 21
4.2. Impairment of the BBB integrity: in vivo permeability measurements 21
4.3. Gene expression changes 21
4.3.1. Gene expression changes suggesting BBB dysfunction 21

4.3.2. Expression levels of genes coding key cytokines involved in atherosclerotic processes 23
4.4. Immunohistochemical staining pattern of key BBB proteins in the hippocampus and cortex of WT and APOB-100 transgenic mice 23
4.5. Cell cultures 25
4.5.1. Cell viability studies 25
4.5.2. Endothelial cell function assays 27
4.5.3. Analysis of endothelial cell morphology 29
4.5.4. Cytokine effects on cultured glial cells 31
4.6. Morphological study of brain microvessels 33
5. Discussion 35
5.1. *In vivo* experiments 35
5.2. *In vitro* and *ex vivo* experiments 36
5.2.1. Primary brain microvascular endothelial cell cultures 36
5.2.1.1. Functional characteristics 36
5.2.1.2. Morphological characteristics 39
5.2.2. Glial cell cultures 40
5.2.3. *Ex vivo* experiments – isolated brain microvessels 41
6. Summary 45
7. Conclusions 46
8. Acknowledgments 47
9. References 48

LIST OF PUBLICATIONS

Publications related to the subject of the thesis:

I. Barabási B, Barna L, Santa-Maria AR, Harazin A, Molnár R, Kincses A, Vigh JP, Dukay B, Sántha M, Tóth ME, Walter FR, Deli MA, Hoyk Z. Role of interleukin-6 and interleukin-10 in morphological and functional changes of the blood-brain barrier in hypertriglyceridemia. Fluids Barriers CNS. 2023 Mar 7;20(1):15. doi: 10.1186/s12987-023-00418-3 ($IF_{2022-2023}$: 7.3, Journal Ranking: D1)

II. Hoyk Z, Tóth ME, Lénárt N, Nagy D, Dukay B, Csefová A, Zvara Á, Seprényi G, Kincses A, Walter FR, Veszelka S, Vígh J, **Barabási B**, Harazin A, Kittel Á, Puskás LG, Penke B, Vígh L, Deli MA, Sántha M. Cerebrovascular Pathology in Hypertriglyceridemic APOB-100 Transgenic Mice. Front Cell Neurosci. 2018 Oct 25;12:380. doi: 10.3389/fncel.2018.00380. (IF_{2018}: 3.9, Journal Ranking: Q1)

Publications not related to the subject of the thesis:

I. Barabási B, Csondor A, Martín-Pozas T, Pulupa Sánchez AM, Antalffy G, Siklós L, Gómez-Pinedo U, Párducz Á, Hoyk Z. Effect of axotomy and 17β-estradiol on P2X7 receptor expression pattern in the hypoglossal nucleus of ovariectomized mice. Neuroscience. 2016 Apr 5;319:107-15. doi: 10.1016/j.neuroscience.2016.01.049.
(IF_{2016}: 3.277, Journal Ranking: Q1)

II. Dukay B, Walter FR, Vigh JP, **Barabási B**, Hajdu P, Balassa T, Migh E, Kincses A, Hoyk Z, Szögi T, Borbély E, Csoboz B, Horváth P, Fülöp L, Penke B, Vígh L, Deli MA, Sántha M, Tóth ME. Neuroinflammatory processes are augmented in mice overexpressing human heat-shock protein B1 following ethanol-induced brain injury. J Neuroinflammation. 2021 Jan 10;18(1):22. doi: 10.1186/s12974-020-02070-2. (IF_{2021}: 9.589, Journal Ranking: Q1)

Cumulative impact factor: 24.066

LIST OF ABBREVIATIONS

APOB: Apolipoprotein B

AQP4: Aquaporin 4

BBB: Blood-brain barrier

BEC: Brain endothelial cell

BSA: Bovine serum albumin

CNS: Central nervous system

DHA: Docosahexaenoic acid

DMEM: Dulbecco's modified Eagle's medium

GFAP: Glial fibrillary acidic protein

GLUT: Glucose transporter

GSK3β: Glycogen synthase kinase-3 beta

IBA: Ionized calcium binding adaptor molecule

IL: Interleukin

LDL: Low-density lipoprotein

LOX: Lectin-like oxLDL (oxidized low-density lipoprotein) receptor

LRP: Low density lipoprotein receptor-related protein

MEOX2: Mesenchyme homeobox protein 2

MFSD2A: Major facilitator superfamily domain-containing protein 2a

NF-κB: Nuclear factor kappa B

PB: Phosphate buffer

PBS: Phosphate buffered saline

P-gp: P-glycoprotein

S100B: S-100 protein family calcium-binding protein B

SF: Sodium fluorescein

TEER: Transendothelial electrical resistance

TJ: Tight junction

TJP: Tight junction proteins

TNF: Tumour necrosis factor

VLDL: Very low density lipoprotein

WT: Wild type

ZO-1: Zonula occludens-1

1. Introduction

Hyperlipidemia is a common pathological condition, which is closely linked to cardio- and cerebrovascular diseases, and paves the way to the development of neurodegenerative diseases. Elevated levels of cholesterol and triglycerides in the blood are reflected by high concentration of low-density lipoprotein (LDL) (Figure 1) particles. Since lipids are not soluble in water, they are transported in the blood packed into lipoprotein complexes, which are made of a hydrophilic outer layer and a hydrophobic inner core (Segrest et al., 2001). Cholesterol esters and triglycerides that are being transported in the blood reside in the hydrophobic core, while the outer hydrophilic shell contains phospholipid membranes and special proteins, known as apoproteins (Segrest et al., 2001). Apoproteins are responsible for stabilizing lipoprotein complexes and binding them to their receptors. Different lipoproteins contain different apoproteins. The major protein component of LDL and very low density lipoproteins (VLDLs) is apolipoprotein B-100 (APOB-100), which is a large, 512 kDa glycoprotein (Chan, 1992; Lénárt et al., 2015). Consequently, APOB-100 levels are related to LDL concentration.

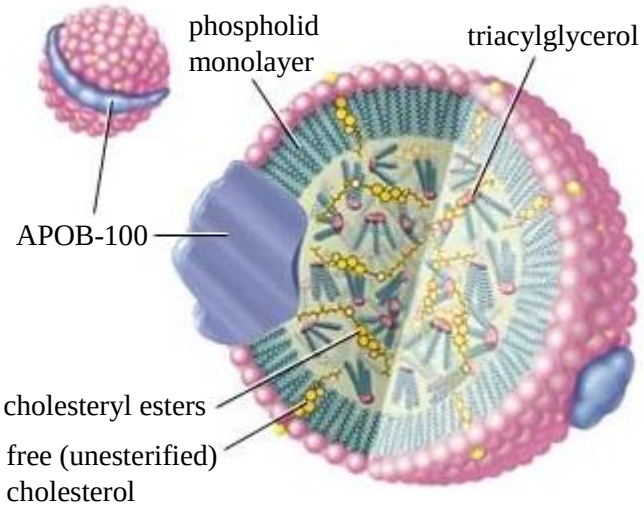

Figure 1. Molecular composition of the low-density lipoprotein (LDL) complex. The triglyceride and cholesterol ester core of LDL is surrounded by phospholipids, free cholesterol and apolipoprotein B-100. (Encyclopædia Britannica, Inc. 2007. https://www.britannica.com/science/ester-chemical-compound).

Elevated LDL levels are closely linked to the development of atherosclerosis (Ross and Harker, 1976), because LDL particles are susceptible to oxidative processes in the subendothelial space (Schwenke and Carew, 1989; Schissel et al., 1998). Oxidized LDL induces the expression of cell adhesion molecules on endothelial cell surfaces, leading to monocyte recruitment. Monocytes, in turn, enter the subendothelial space where they

progressively differentiate into macrophages, which take up oxidized LDL and subsequently are converted into foam cells. Smooth muscle cells of the arterial wall may also accumulate modified lipids contributing to both conversion to foam cell and fibrous cap formation (Glass and Witztum, 2001). Adhesion molecules and chemokines are involved not only in monocyte recruitment but also participate in guiding T lymphocytes into atherosclerotic plaques. The immune cells present in atherosclerotic lesions interact with each other and secrete a broad range of cytokines with pro- and anti-inflammatory effects (Glass and Witztum, 2001).

Macrophages and smooth muscle cells in atherosclerotic lesions produce interleukin (IL)-6, a pleiotropic cytokine, which is associated with endothelial dysfunction (Seino, 1994; Kishikawa, 1993; Ridker, 2016). Vascular cells may promote inflammatory processes by synthesizing tumour necrosis factor (TNF)-α, IL-1β, IL-6, IL-8 and IL-15, and may exert anti-inflammatory action mainly by transforming growth factor-β production. Another cytokine playing an anti-inflammatory role in atherosclerosis is IL-10, which is primarily produced by macrophages and T and B lymphocytes (Tedgui and Mallat, 2006) and in very small quantities by brain capillary endothelial cells (Verma et al., 2006). Due to the prolonged expression of a wide repertoire of pro-inflammatory cytokines, atherosclerosis is considered a chronic inflammatory disease (Tedgui and Mallat, 2006). Hyperlipidemia is associated with systemic inflammation even without cardiovascular pathologies. Patients with high triglyceride levels have an increased capacity to produce TNF-α and IL-6 (Jonkers et al., 2002). Systemic inflammation also affects the brain and its vasculature, and damages their functions (Farkas et al., 1998).

In order to study the pathological alterations induced by hyperlipidemia, an animal model was established by the research group headed by Miklós Sántha, PhD, DSc, in 2005, in the Biological Research Centre. This animal model is a transgenic mouse line, which overexpresses the human apolipoprotein (APO) B-100 protein in different tissues such as the liver, heart and brain (Bjelik et al., 2006; Csont et al., 2007; Lénárt et al., 2012).
APOB-100 transgenic mice show significantly elevated serum triglyceride and cholesterol level when fed with normal chow and cholesterol rich diet, respectively (Csont et al., 2007). The plasma membrane of brain endothelial cells isolated from these transgenic animals is characterized by increased rigidity (Lénárt et al., 2015). Moreover, various neurodegenerative processes occur in the brain of hypertriglyceridemic APOB-100 transgenic mice. Widespread neuronal cell death and apoptosis of cortical and hippocampal

neurons was detected in this model (Lénárt et al., 2012). Synaptic dysfunction in the hippocampal region of APOB-100 transgenic mice using electrophysiology and hyperphosphorylation of the tau protein (primarily at Ser262, Ser396, Ser199/202, Ser404 phosphosites) were also shown (Lénárt et al., 2012). As a consequence of the extended neurodegeneration a pronounced enlargement of brain ventricles in transgenic brains was detected using MRI, which was transgene dose-dependent (Bereczki et al., 2008). APOB-100 overexpression is also linked to an increased level of lipid peroxidation in cortical and hippocampal brain regions and to impaired cognitive function (Löffler et al., 2013).

The observed pathological changes caused by hyperlipidemia are well-known characteristics of Alzheimer's disease. Several neurodegenerative processes, including Alzheimer's disease, Parkinson's disease and multiple sclerosis are related to impaired cerebrovascular functions, including the dysfunction of a dynamic interface between the brain parenchyma and the circulating blood, known as the blood-brain barrier (BBB; Benett et al., 2010; Burgess et al., 2006; Martins et al., 2009; Sweeney et al., 2018; Zlokovic, 2011).

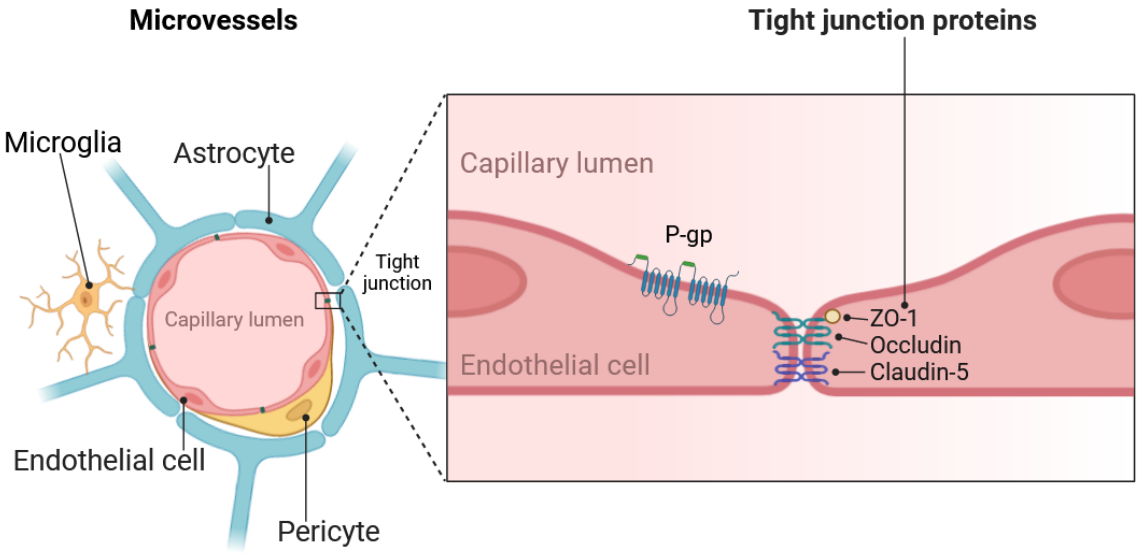

Figure 2. General structure of the Blood-Brain Barrier (BBB).

The cellular components of the mature BBB are non-fenestrated endothelial cells, the basement membrane and the surrounding pericytes and astroglial endfeet (Abbott et al., 2010). The endothelial cells adhere tightly to one another, through junctional structures

termed tight junctions (TJs), which restrict the paracellular permeability of the BBB (Abbott et al., 2010; Wolburg et al., 2009). The endothelial TJs are made of integral transmembrane proteins (occludin and predominantly claudin-5), adaptor cytoplasmic proteins (ZO-1, -2), and by adherens junction proteins (Abbott et al., 2010) (Figure 2). The exchange of solutes across the BBB occurs in a controlled manner via transcellular transport systems, including carrier-mediated and receptor-mediated transport, adsorptive mediated transcytosis and active efflux transport (Campos-Bedolla et al., 2014; Zlokovic, 2011). The chemoprotection of the brain by the efflux of potentially toxic lipophilic/amphiphilic molecules is mediated by ATP-binding cassette transporters, like the multidrug resistance transporter P-glycoprotein (P-gp/ABCB1), which shows reduced expression in systemic inflammation (Hartz, 2006) and impaired function in neurodegenerative diseases (Sweeney et al., 2018).
BBB properties highly depend on the cross-talk between brain capillary endothelial cells, astroglial processes and pericytes. In the adult, the BBB is stabilized by perivascular cells (Zhao et al., 2015). Astroglial processes develop microvascular endfeet that cover the vasculature forming part of the BBB (Mathiisen et al., 2010). These astrocytic perivascular endfeet contain the water channel aquaporin 4 (AQP4) in tenfold higher densities than non-endfoot astrocyte membranes (Wolburg et al., 2009). AQP4 channels permit bidirectional water flow between brain and blood driven by osmotic gradients contributing to the maintenance of ion and volume homeostasis in the CNS under physiological conditions. During pathologic events, like neuroinflammation, however, AQP4 protein expression is decreased in the perivascular endfeet indicating impairment of BBB function (Wolburg et al., 2009).

Neuroinflammation involves a complex interplay of pro- and anti-inflammatory cytokines, which are produced primarily by immune cells. However, other cell types, like cells of the neurovascular unit, such as astrocytes and pericytes, may also participate in cytokine generation under control conditions. Astrocytes and pericytes are able to produce pro-inflammatory cytokines including TNF-α and IL-6, two important cytokines playing a role in atherosclerosis (Banks et al., 2018). Brain endothelial cells, in contrast, do not produce TNF-α nor IL-6 in a healthy microenvironment, but they react to challenges, such as LPS stimulation, which induces endothelial TNF-α and IL-6 production (Banks et al., 2018). Astroglia and endothelial cells may participate not only in IL-6 production, but their function can also be modulated by IL-6, since these cells express IL-6 receptors (Erta et al., 2012; Database of gene expression in adult mouse brain and lung vascular and perivascular cells;

Vanlandewijck et al., 2018; He et al., 2018;). Moreover, astroglia and endothelial cells can respond to the anti-inflammatory cytokine IL-10, too (Burmeister and Marriott, 2018).

Microglia cells, another type of glia, are located not only in the brain parenchyma, but also in the perivascular niche, between the vascular wall and astrocytic endfeet. Microglia can make direct contacts with the cells of the BBB including endothelial cells and regulate cerebral blood flow (Császár et al., 2022). Microglia cells express receptors for various cytokines produced by cellular components of the BBB during atherosclerosis, including IL-6 (Erta et al., 2012), which may contribute to microglia activation. Microglia reactions, in turn, may involve release of pro-inflammatory cytokines TNF-α and IL-1β leading to BBB impairment (da Fonseca et al., 2014). Pro-inflammatory cytokines including TNF-α and IL-6 can be produced not only within the central nervous system, but they can reach the brain vasculature originating from peripheral inflammatory conditions, resulting in increased BBB permeability (Farkas et al., 1998). Microglial production of pro-inflammatory cytokines may be inhibited by IL-10 (Lobo-Silva et al., 2016) an anti-inflammatory cytokine synthesized by immune cells infiltrating atherosclerotic plaques (Tedgui and Mallat, 2006).

Inflammatory processes are involved in several pathologies, including the development of neurodegenerative diseases. TNF-α and IL-1 are reported to promote the synthesis of amyloid β (Brosseron et al., 2014; Decourt et al., 2017; Koenigsknecht-Talboo and Landreth, 2005, Rubio-Perez and Morillas-Ruiz, 2012), but the cytokine playing an essential role in atherosclerosis, IL-6, is also present at high concentration in the serum of Alzheimer's disease patients (Brosseron et al., 2014). Moreover, IL-6 is considered a key factor in the pathogenesis of multiple sclerosis, too (Petkovic and Castellano, 2016).

Neurodegenerative conditions can be observed in APOB-100 transgenic mice that originally served as a model of human atherosclerosis. It suggests that APOB-100-induced vascular changes may result in neurodegenation. However, the details of the link between vascular inflammation and neurodegeneration, and especially the role played by the BBB in this process, are largely unexplored.

2. Aim of the study

Our aim was to study BBB related structural and functional changes in APOB-100 transgenic mice that may reveal pathological processes triggered by hypertriglyceridemia, and leading to neurodegeneration. Regarding molecular and cellular mechanisms, we aimed to highlight the effects of IL-6, a pro-inflammatory cytokine which is involved in atherosclerosis, on endothelial and glial cell characteristics, and the possible protective action of an anti-inflammatory cytokine, IL-10. The specific questions of the research projects were the following:

In APOB-100 mice

- are there changes in BBB permeability for small and large marker molecules in the brain cortex and hippocampus?
- does the expression of key BBB genes and cytokines IL-6 and IL-10 change in the microvessel fraction?
- are there any changes in occludin, claudin-5 and P-gp immunostaining in brain cortex and hippocampus?

Are there differences in the effects of IL-6 and IL-10

- on brain endothelial growth, viability and density from WT and APOB-100 mice?
- on the permeability and efflux pump activity of a BBB co-culture model from WT and APOB-100 mice?
- on occludin, claudin-5 and P-gp immunostaining of brain endothelial cells from WT and APOB-100 mice?
- on microglial and astroglial cell density of cultures from WT and APOB-100 mice?

3. Materials and Methods

3.1. Materials

All reagents were purchased from Merck (Budapest, Hungary) except for those specifically mentioned.

3.2. Animals

Mice were housed in groups of two to three under standard conditions (24 °C, 12 h light-dark cycle) with food and water available *ad libitum*. Animals were maintained on a regular rodent chow diet. The mouse strain overexpressing the human APOB-100 protein was established by the group of Miklós Sántha (Bjelik et al., 2006) and maintained on a C57BL/6 genetic background in a hemizygous form. Breeding of the transgenic mouse strain was approved by the regional Animal Research Ethics Committee (Csongrád county, Hungary; project license: XVI./2724/2017). All animals were handled in accordance with approved procedures as defined by the EU Directive 2010/63/EU. In order to determine the genotype of hemizygous APOB-100 animals and wild type (WT) littermates, DNA from tail biopsies of 2-, or 10-day-old pups was purified, and the presence of the transgene was detected by PCR, using primers for the 5' promoter region of the human APOB-100 gene.

Table 1. Age and number of animals used in the studies.

Experiment	Age of animals (months)	Number of animals/group
Serum triglyceride measurement	7, 9 and 12	5
BBB permeability *in vivo*	6	10
BBB permeability *in vitro*	6-7	6
Microvessel RT-PCR	7	4
Cortex, hippocampus RT-PCR	7	4
Fluorescence intensity analysis	6-7	5
Primary brain endothelial cell isolation	6-7	6
Brain microvessel isolation	6-7	6
Primary glial cell isolation	3-4 day old	6

3.3. *In vivo* studies

3.3.1. Serum triglyceride measurement

Serum triglyceride levels in 7, 9, and 12-month-old APOB-100 transgenic (n = 5) and WT mice (n = 5) fed on a normal chow diet were measured using a colorimetric assay (Table 1). Blood samples were collected through cardiac puncture under terminal anesthesia. After clot formation samples were centrifuged at 4 °C, 1000 × g for 10 min, then serum was removed

and stored at -80 °C until use. Serum triglyceride levels were measured in triplicate using a commercially available enzymatic colorimetric assay kit (Diagnosticum Ltd., Budapest, Hungary) according to the manufacturer's instructions. Test accuracy was monitored using Standard Lipid Controls (Diagnosticum Ltd., Budapest, Hungary). Absorbance of the produced purple color product was measured at 560 nm using a microplate reader (Multiskan FC, Thermo Scientific, United States). Values were expressed in mmol/liter.

3.3.2. *In vivo* permeability measurement of the BBB

Permeability for sodium fluorescein (SF, Mw: 376 Da), a marker of paracellular flux, and Evans blue (EB, Mw: 67 kDa), a tracer which binds to serum albumin (Patterson et al., 1992), was measured as described in detail earlier (Veszelka et al., 2003). Six-month-old WT and transgenic mice (n = 10 animals/group) (Table 1) were given a solution of both dyes (2%, 5 ml/kg) in an iv. injection to the tail vein for 1 h, and at the end of the experiments, the animals were perfused with 25 ml phosphate-buffered saline (PBS) for 15 min. Samples from two brain regions, cerebral cortex and hippocampus, were collected, weighed and stored at −80°C. Tissue pieces were homogenized in 650 µl PBS, then 650 µl of cold, 50% w/v, freshly prepared trichloroacetic acid was added and samples were centrifuged again with 10,000 × g for 12 min at 4 °C. Dye concentrations were measured in supernatants by a PTI spectrofluorimeter (T-format, Quanta Master QM-1; Photon Technology International). Five hundred µl of the supernatants were diluted in ethanol (1:3) than emission of Evans blue was measured at 650 nm after excitation at 600 nm wavelength. For SF measurement 500 µl supernatants were diluted in distilled water (1:3) then 100 µl 10N NaOH was added to each sample. Emission of fluorescein was measured at 510 nm after excitation at 492 nm wavelength. BBB permeability was expressed as ng tracer/g brain tissue.

3.3.3. Immunohistochemistry and confocal microscopy

Standard immunofluorescence protocols were applied. Mice (7-8-months-old; Table 1) were terminally anesthetized with sodium pentobarbital (150 µg/g, i.p.), transcardially perfused with 0.9% sodium chloride dissolved in 0.01 M PB, pH 7.4, followed by 3% paraformaldehyde in 0.1 M PB, pH 7.4. Brains were removed and postfixed for 4 h in the same fixative. Following fixation the brain samples were washed in 0.1 M PB, pH 7.4, and cryoprotected in 30% sucrose until saturation. Then, 30-µm-thick, hippocampus and frontal cortex containing coronal sections were cut on a cryostat (Floorstanding Cryostat MNT;

Slee, Mainz, Germany), collected in 0.1 M PB, pH 7.4 containing 0.01% sodium azide (Fluka) (w/v) and were stored at 4 °C. Antigen retrieving for claudin-5 and occludin immunostaining was performed with 0.5 % Triton X-100 in PBS for 10 min, followed by an incubation in protease type XIV (1 µg/ml) dissolved in $CaCl_2$ (1 mg/ml) for 7 min. Antigen retrieving for the P-gp primary antibody used included only Triton X-100 treatment at concentrations based on our preliminary experiments (0.5% for P-gp). Primary antibodies used were rabbit anti-claudin-5, rabbit anti-occludin (Thermo Fisher Scientific, Waltham, MA, United States) and mouse anti-Pgp (Merck Millipore, Burlington, MA, United States) (Table 2). Appropriate secondary antibodies conjugated with DyLight 488 (Invitrogen, Life Technologies, USA) and Alexa Fluor 594 (Invitrogen, Life Technologies, USA) were applied. Sections were counterstained with DAPI, coverslipped with Confocal Matrix R (Micro Tech Lab, Graz, Austria) and examined with a confocal laser scanning microscope (Olympus Fluoview FV1000, Olympus Life Science Europa GmbH, Hamburg, Germany). Images of 512×512 px were captured using the following microscope configuration: objective lens: UPLSAPO 60x, numeric aperture 1.35; sampling speed: 8 µs/pixel; scanning mode: sequential unidirectional. In order to obtain high resolution (1024 × 1024 px) images, Yokogawa W1/Olympus IX83-based spinning disk confocal microscope was also used for imaging immunostaining using excitation and detection parameters optimized for DyLight 488 anti-mouse, Alexa Fluor 594 anti-rabbit and DAPI. For imaging 405nm (for DAPI), 488 nm (for DyLight 488 anti-mouse) and 561 nm (for Alexa Fluor 594 anti-rabbit) laser excitation and 60× objective were used.

Table 2. List of antibodies used in immunohistochemistry.

Antibody name	Vendor	Catalogue number	Host organism	Concentrations	Antibody registry ID
anti-claudin-5	Sigma	SAB4502981	rabbit	0.625 µg/ml	AB_10753223
anti-occludin	ThermoFisher Scientific	71-1500	rabbit	0.2 µg/ml	AB_2533977
anti-Pgp	Millipore	517310	mouse	3 µg/ml	AB_564389
anti-rabbit-A594	Invitrogen	A21207	donkey	1 µg/ml	AB_141637
anti-mouse-DyLight 488	Invitrogen	35502	goat	1 µg/ml	AB_844397

3.4. *In vitro* studies

3.4.1. Brain endothelial cell cultures

The primary cultures of brain endothelial cells (BECs) were prepared from 6-7-month-old WT and APOB-100 transgenic mice (Lénárt et al., 2015). For each isolation 3 male and 3

female mice were used in both the WT and the APOB-100 groups (n = 6/group; Table 1). Forebrains were collected in ice-cold sterile PBS; meninges were removed, grey matter was minced by scalpel into 1 mm^3 pieces and digested with 10 mg/ml collagenase II and 1 mg/ml DNase I in Dulbecco's modified Eagle's medium (DMEM)/F12 for 50 min at 37 °C. Microvessels were separated from myelin containing elements by centrifugation (1000× g, 20 min) in 20% bovine serum albumin (BSA)-DMEM and further digested with 10 mg/ml collagenase-dispase (Roche, Basel, Switzerland) and 1mg/ml DNase I in DMEM/F12 for 35 min at 37 °C. Then they were washed twice in DMEM/F12 before plating on collagen type IV and fibronectin-coated (100 μg/ml each) dishes, 6 well plates (Corning Costar Co., Lowell, MA, USA) or cell culture inserts (Transwell clear, 1 cm^2; pore size of 0.4 μm; Corning Costar Co.). Cultures were maintained in DMEM/F12 supplemented with 15% plasma-derived bovine serum (PDS; First Link, Wolverhampton, UK), 1 ng/ml basic fibroblast growth factor (Roche) and 100 μg/mL heparin. During the first 2 days, the culture medium contained puromycin (4 μg/ml) in order to selectively remove P-gp-negative contaminating cells (Perrière et al., 2005). Cultures reached confluency within a week and were used for experiments. To induce BBB characteristics, BECs were co-cultured with mouse astroglial cells. The resulting double co-culture model was used for permeability studies and transendothelial electrical resistance measurements (Deli et al., 2005; Veszelka et al., 2007).

3.4.2. Mixed glial cell cultures

Primary mouse glial cells were isolated and cultured as described in our earlier publication (Lénárt et al., 2015). Briefly, 3 male and 3 female mice were used in both the WT (n = 6) and the APOB-100 group (n = 6) for each isolation (Table 1). Forebrains were obtained from 3 or 4-day-old WT and APOB-100 transgenic mice and placed into ice-cold PBS. Meninges were removed and little pieces of cortices were pipetted into 50-ml tubes and then the tissue was mechanically dissociated by using a long and thin needle (21G 4 ¾, Braun, Germany). Isolated cells were plated onto uncoated T25 flasks (Corning Costar Co.) and cultured in low-glucose DMEM (Thermo Fisher Scientific, Waltham, Massachusetts, USA), which contained 10% fetal bovine serum (Sera Plus, Pan Biotech, Aidenbach, Germany) and gentamycin (50 μg/ml). Glial cells were cultured until confluency with medium change every 2 days. Then glial cells were seeded onto poly-L-lysine-coated coverslips placed into 24-well plates and cultured with medium change every 3 days. Cultures reached confluency in 5-7 days. Then they were treated with cytokines, fixed and immunostained. Confluent cell

layers consisted of 57% astrocyte and 43% microglia in WT, and 49% astrocyte and 51% microglia in APOB-100 glia cultures.

3.4.3. Endothelial cell viability assays

Kinetics of the viability of BECs was observed by a real-time impedance measurement (RTCA-SP, Agilent, Santa Clara, CA, USA) as described previously (Walter et al., 2022). Impedance correlates linearly with cell number, adherence, growth and viability. BECs were grown on golden electrodes of 96-well E-plates (Agilent) in a CO_2 incubator at 37 °C for 5 days. Then the cells were treated with cytokines at 10 or 50 ng/ml concentration in 3 combinations: IL-6, IL-10 and IL-6+IL-10. Effects of treatments were monitored for 24 h.

3.4.4. Cytokine treatments

Treatment of primary BECs and glial cells was carried out in their respective culture medium for a maximum treatment period of 24 h. Cortical microvessels were treated immediately after isolation for a period of 1 hour. For these treatments, both IL-6 and IL-10 were used at 50 ng/ml concentration.

3.4.5. BBB functional assays

3.4.5.1. Permeability measurements on BBB co-culture model

Permeability tests using the small molecular marker SF were carried out on an in-contact type double co-culture BBB model with primary glial cells when high transendothelial electrical resistance (TEER) values were recorded. After applying IL-6, IL-10 and IL-6+IL-10 in combination (both cytokines at 50 ng/ml concentration) for 24 h in the luminal compartment, the test was conducted as described previously (Walter et al., 2022). The concentration of the SF marker molecule in samples from the upper and lower compartments was determined with a microplate reader (excitation at 440 nm, emission at 525 nm; BMG Fluostar Optima; BMG Labtech, Ortenberg, Germany). Flux across coated, cell-free inserts was also measured. Endothelial permeability coefficients (P_e) were calculated from clearance values of tracers as described in detail in our previous publication (Lénárt et al., 2015).

3.4.5.2. Transendothelial electric resistance on BBB co-culture model

TEER representing the permeability of TJs for sodium ions in culture conditions was measured by an EVOM resistance meter (World Precision Instruments Inc., Sarasota, FL, USA) using STX-2 electrodes, and expressed relative to the surface area of the endothelial

monolayer ($\Omega \times cm^2$) as described in our earlier publication (Lénárt et al., 2015). The background TEER value of inserts without cells (21 $\Omega \times cm^2$) was subtracted from the measured values.

3.4.5.3. P-glycoprotein activity on BBB monoculture model

P-gp/ABCB1 activity was determined by measuring the cellular accumulation of the efflux pump ligand rhodamine 123 (R123). BECs were seeded in 24-well plates and incubated in Ringer-HEPES containing 10 µM rhodamine 123 (R123) for 1 h at 37 °C after cytokine treatments. Cyclosporine A (1.6 µM), which blocks P-gp and breast cancer-resistant protein/ABCG2 was used as a reference inhibitor molecule. Following cytokine treatments and incubation with R123, BEC monolayers were washed 3 times with ice-cold PBS, then solubilized in 0.1 M NaOH. Fluorescence intensity indicating intracellular R123 concentration was measured in a 96-well plate (Fluostar Optima; excitation: 485 nm, emission: 520 nm).

3.4.6. Immunocytochemistry and confocal microscopy

The immunostaining pattern of claudin-5, occludin, ZO-1 and P-gp was studied in primary BECs isolated from WT and APOB-100 transgenic mice. Cells were fixed with ice-cold acetone-methanol for 2 min, then non-specific binding was blocked with 1% BSA in PBS at room temperature during 1h. Cells were incubated with primary antibodies shown in Table 3 overnight at 4 °C, which was followed by a 1h incubation with the corresponding secondary antibodies (A594-conjugated donkey anti-rabbit, A488-conjugated goat anti-mouse (Thermo Fisher Scientific, MA, USA) and Cy3-labeled sheep anti-rabbit, as shown in Table 3). Cellular nuclei were stained with Hoechst 33342 (Thermo Fisher Scientific) at a concentration of 1 µg/ml. The samples were mounted (Fluoromount-G; Southern Biotech, AL, USA), then examined using a Spinning Disk Confocal Microscope (Zeiss, Germany).

Astroglia and microglia were immunolabeled to visualize GFAP, S100B, AQP4 and Iba-1 expression, respectively. Glial cells were fixed with 3% paraformaldehyde and permeabilized with 0.2% Triton X-100 in PBS for 10 min. Non-specific binding of antibodies was blocked with 3% BSA in the case of S100B+AQP4 co-staining, and with 2% normal horse serum and 5% normal goat serum for Iba-1+GFAP co-labeling. Glial cells were incubated with primary antibodies (Table 3) overnight at 4 °C, followed by incubation with the corresponding secondary antibodies for 1h (A488-labeled donkey anti-goat (Thermo Fisher Scientific), DyLight 549-conjugated goat anti-mouse (Jackson

ImmunoResearch Europe Ltd., Cambridgeshire, UK), A594-conjugated donkey anti-rabbit (Thermo Fisher Scientific), as shown in Table 3. Hoechst dye 33342 was used for nuclear staining at a concentration of 1 µg/ml. After mounting the samples (Fluoromount-G; Southern Biotech), the immunoreactivity was examined using a Leica TCS SP5 confocal laser scanning microscope (Leica Microsystems, Germany).

Table 3. List of antibodies used for immunocytochemistry.

Antibody name	Vendor	Catalogue number	Host organism	Concentrations	Antibody registry ID
Fluorescent immunostaining - Glia cultures (culture purity assessment)					
anti-GFAP	Sigma	G3893	mouse	12.17 µg/ml	AB_477010
anti-Iba1	Abcam	ab5076	goat	0.5 µg/ml	AB_2224402
anti-mouse-A488	Invitrogen	A21202	donkey	1 µg/ml	AB_141607
anti-goat-A488	Invitrogen	A11055	donkey	1 µg/ml	AB_2534102
anti-mouse-Dylight 549	Jackson ImmunoResearch	115-505-003	goat	0.94 µg/ml	-
Fluorescent immunostaining - Cell cultures					
anti-claudin-5	Sigma	SAB4502981	rabbit	0.625 µg/ml	AB_10753223
anti-occludin	Invitrogen	71-1500	rabbit	0.2 µg/ml	AB_2533977
anti-ZO1	Invitrogen	61-7300	rabbit	0.25 µg/ml	AB_2533938
anti-Pgp	Calbiochem	517310	mouse	0.4 µg/ml	AB_564389
anti-Aqp4	Merck	AB3594	rabbit	0.4 µg/ml	AB_91530
anti-Iba1	Abcam	ab5076	goat	0.5 µg/ml	AB_2224402
anti-GFAP	Sigma	G3893	mouse	3.65 µg/ml	AB_477010
anti-S100B	Synaptic System	287011	mouse	0.6 µg/ml	AB_2814881
anti-rabbit-A594	Invitrogen	A21207	donkey	1 µg/ml	AB_141637
anti-mouse-A488	Invitrogen	A11029	goat	1 µg/ml	AB_2534088
anti-rabbit-Cy3	Sigma	C2306	sheep	2.5 µg/ml	AB_258792
anti-goat-A488	Invitrogen	A11055	donkey	1 µg/ml	AB_2534102
anti-mouse-DyLight 549	Jackson ImmunoResearch	115-505-003	goat	0.94 µg/ml	-

A: Alexa Fluor

3.5. *Ex vivo* studies

3.5.1. Brain microvessel isolation

Cortical microvessels were isolated from the brain of 6-7-month-old animals, as described earlier (Szczepkowska et al., 2021). For each isolation 3 male and 3 female mice were used in both the WT and the APOB-100 groups (n = 6/group; Table 1). The forebrains of APOB-100 or WT mice were collected in ice-cold sterile phosphate buffered saline (PBS). Meninges were taken off by rolling brains on a sterile wet filter paper. White matter and the choroid plexus were removed and the tissue was cut into 1 mm^3 pieces by scalpels. Samples then were homogenized in ice-cold Ringer-HEPES buffer (4 ml/g of tissue), and the resulting

homogenates were centrifuged at 2000 *g* for 10 min. After centrifugation the microvessel enriched pellets were resuspended in 17.5% dextran (64-76 kDa) in Ringer-HEPES (118 mM NaCl, 4.8 mM KCl, 2.5 mM $CaCl_2$, 1.2 mM $MgSO_4$, 5.5 mM D-glucose, 10 mM HEPES, pH 7.4) and centrifuged at 4 °C, 4400 g for 15 min. The resulting pellets were suspended in 2 ml Ringer-HEPES buffer containing 1% BSA, while the supernatants were collected and centrifuged once more. The resulting pellets were pooled and passed through nylon meshes with 100 µm and 20 µm pore size. The microvessels retained by the mesh with 20 µm pore size were washed off with 15 ml buffer and centrifuged at 4 °C, 1000 *g* for 10 min. After a second wash in 10 ml buffer (4 °C, 700 *g*, 5 min), microvessels were immediately treated with cytokines.

3.5.2. RNA isolation and quantitative real time PCR

For RNA isolation, forebrains of 8 WT and 8 APOB-100 transgenic mice were used (7 months old; 4 male and 4 female animals/group) (Table 1). Hemispheres of the brains were separated and the left hemispheres were further divided into hippocampal and cortical regions. Right hemispheres were pooled and were used for microvessel isolation as described above. Samples were stored in RNA-later solution (Invitrogen, Life Technologies, USA) at -80 °C until use. Total RNA was isolated from the hippocampal and cortical brain regions and from microvessel samples using an RNA and protein purification kit (Macherey-Nagel, Düren, Germany) according to the manufacturer's instructions. High Capacity cDNA Reverse Transcription Kit (Thermo Fisher Scientific, Waltham, Massachusetts, USA) was used to convert mRNA samples to cDNA. Each reaction mixture contained 15 µL RNA sample (1000 ng in the case of hippocampal and cortical samples, 350 ng for microvessels), 1.5 µL reverse transcriptase, 3 µL primer, 1.2 µL dNTP, 3 µL buffer, 6.3 µL RNase-free water. Parameters for the reverse transcription program were the following: incubation at 25 °C for 10 minutes, reverse transcription at 37 °C for 2 hours, and inactivation at 85 °C for 5 minutes (using MJ Mini - Personal Thermal Cycler, BioRad). The cDNA product was finally diluted 1:20, and was used as a template in the qPCR reaction. For the qPCR reaction, 10 µL cDNA, 1 µL (250nM final) primer mix (forward+reverse), and 10 µL Power SYBR Green PCR Master Mix 2x (Thermo Fisher Scientific, Waltham, Massachusetts, USA) were mixed. Each reaction was performed in a total volume of 20 µL, and was run on a RotorGene 3000 instrument (Qiagen, Hilden, Germany) with the following settings: heat activation at 95 °C for 10 min; followed by 40 cycles of denaturation at 95 °C for 15 s, annealing at 60 °C for 60 s. Melting curve analysis was performed between 50-95 °C to verify the specificity

of the amplification. Primer sequences used in qPCR reactions are listed in Table 4, of which the mouse *Gapdh* (for hippocampal and cortical samples) and *Actb* (for microvessel samples) genes served as an internal control for normalization. Relative gene expression levels were calculated using the ΔΔCt method.

Table 4. Gene-specific primers for qPCR analysis.

Gene	Forward primer	Reverse primer
Gapdh	GGGTTCCTATAAATACGGACTGC	CCATTTTGTCTACGGGACGA
Actb	CTAAGGCCAACCGTGAAAAG	ACCAGAGGCATACAGGGACA
IL6	GCTACCAAACTGGATATAATCAGGA	CCAGGTAGCTATGGTACTCCAGAA
IL10	CAGAGCCACATGCTCCTAGA	TGTCCAGCTGGTCCTTTGTT

3.5.3. Immunohistochemistry on isolated brain microvessels and confocal microscopy

Isolated brain microvessels were fixed with 3% paraformaldehyde immediately after cytokine treatment, and the expression pattern of key BBB proteins claudin-5, occludin, ZO-1, P-gp and AQP4 was analyzed using immunocytochemistry. Microvessels were permeabilized and non-specific binding was blocked with 0.2% Triton X-100 and 2% normal serum in PBS for 10 min. Then microvessels were incubated overnight at 4°C with primary antibodies at dilutions shown in Table 5. The next day, microvessels were incubated for 50 min (Table 5) with the corresponding secondary antibodies, i.e. A594-conjugated donkey anti-rabbit and A488-conjugated goat anti-mouse (Thermo Fisher Scientific), as shown in Table 5. Cellular nuclei were stained with Hoechst 33342 (Thermo Fisher Scientific) at a concentration of 1 µg/ml. Between incubations microvessels were washed three times with PBS. The staining patterns were examined with a Spinning Disk Confocal Microscope (Zeiss, Germany).

Table 5. List of antibodies used in immunohistochemistry on isolated brain microvessels.

Antibody name	Vendor	Catalogue number	Host organism	Concentrations	Antibody registry ID
Fluorescent immunostaining - Microvessels					
anti-claudin-5	Sigma	SAB4502981	rabbit	0.625 µg/ml	AB_10753223
anti-occludin	Invitrogen	71-1500	rabbit	0.2 µg/ml	AB_2533977
anti-ZO1	Invitrogen	61-7300	rabbit	0.25 µg/ml	AB_2533938
anti-Pgp	Calbiochem	517310	mouse	0.4 µg/ml	AB_564389
anti-Aqp4	Merck	AB3594	rabbit	0.4 µg/ml	AB_91530
anti-rabbit-A594	Invitrogen	A21207	donkey	1 µg/ml	AB_141637
anti-mouse-A488	Invitrogen	A11029	goat	1 µg/ml	AB_2534088
anti-rabbit-Cy3	Sigma	C2306	sheep	2.5 µg/ml	AB_258792
anti-mouse-DyLight 549	Jackson ImmunoResearch	115-505-003	goat	0.94 µg/ml	-

3.6. Image analysis

Fluorescence intensity of immunolabeling in BEC cultures was quantified using the ImageJ program. The background intensity was subtracted from integral intensity values of immunofluorescent signals. The resulting immunofluorescence values were normalized to the number of pixels showing immunolabeling. The number of images analyzed was n = 5-15/treatment group for each staining.

Cell density was determined by nucleus number/10000 μm^2. In the case of mixed glial culture, astroglia and microglia nuclei were counted separately. The WT control was considered 100%, all the other treatment groups and transgenic groups were normalized to it. In order to assess the ratio of microglia and astroglia in the mixed culture, their cell numbers in each picture were compared and their ratio was calculated (n= 8-10).

The immunolabeling in isolated microvessels was quantified by calculating the area fraction of immunostained structures in microvessels using Matlab software. Images were divided into smaller fractions by an expert in immunohistochemistry using freehand drawing in order to get images containing one immunolabeled microvessel only and discard signals coming from tissue debris. Then, low threshold was set for the binarization of the immunolabeling to highlight the whole surface of the microvessel. The pixel numbers of these segments gave the area of the microvessels on each image. Next, the global threshold of the specific immunostaining was determined using Otsu's method, resulting in binary images of the immunolabeled structures (Otsu, 1979). The pixel numbers of these binary images represented the area of the labeled structures. Each area of immunostained structure was normalized to the corresponding total microvessel area. The number of images analyzed was n = 5-15/treatment group for each staining.

3.7. Statistical analysis

GraphPad Prism 5.0 software (GraphPad Software Inc. LaJolla, CA, USA) was used for statistical analysis. Gaussian distribution of the data was tested with the Kolmogorov–Smirnov normality test. Data showing Gaussian distribution were analyzed with two-way analysis of variance followed by Bonferroni post hoc test. Data showing no Gaussian distribution were analyzed with Kruskal–Wallis and Dunn's multiple comparison tests. The level of statistical significance was taken as $p < 0.05$. Results are presented as means ± SEM.

4. Results

4.1. Chronic hypertriglyceridemia in APOB-100 transgenic mice

In order to check the effect of the expression of the human APOB-100 gene in mice on serum lipids, triglyceride concentrations were measured in blood samples of 7-, 9- and 12-month-old WT and APOB-100 transgenic mice. Significantly higher triglyceride concentrations were detected in transgenic compared to WT animals at every time point indicating chronic hypertriglyceridemia in APOB-100 transgenic mice (Figure 3A).

4.2. Impairment of the BBB integrity: in vivo permeability measurements

Next, we examined the functional characteristics of the BBB in living animals, focusing on the permeability of two marker molecules which differ in size: the small molecule SF, which provides information on paracellular flux, and the large molecule Evans blue-albumin, a marker of transcellular permeability. We measured a significant increase in BBB permeability ($p < 0.05$) for SF in the hippocampal region of transgenic mice, while alteration in the extravasation of the large serum protein albumin showed a non-significant trend. However, there was no obvious change in the permeability for either of the markers in the cortex of transgenic mice compared to WT littermates (Figure 3B).

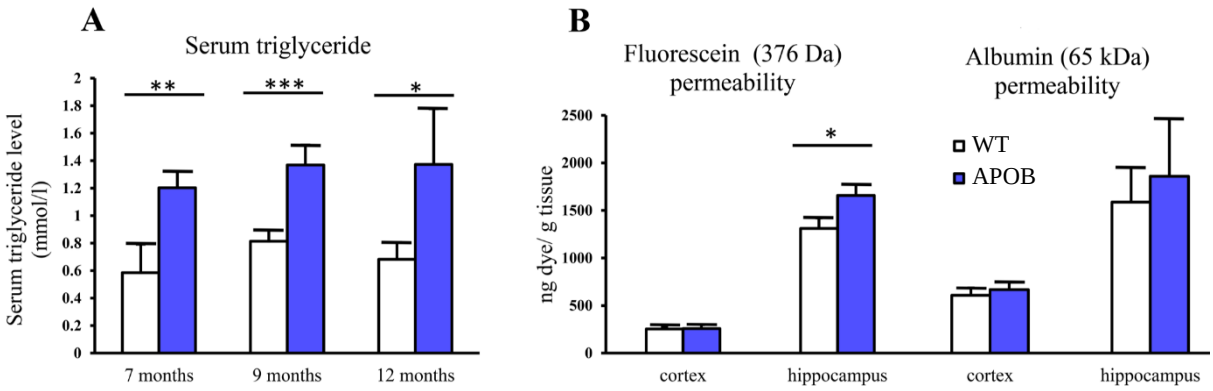

Figure 3. (A) Serum triglyceride levels and (B) BBB permeability for fluorescein and albumin in the brain of hypertriglyceridemic APOB-100 transgenic (APOB) and wild-type (WT) mice.

4.3. Gene expression changes

4.3.1. Gene expression changes suggesting BBB dysfunction

The observed increase in BBB permeability suggested that hypertriglyceridemia contributed to pathological conditions that may lead to changes in gene and/or protein expression in brain microvessels. The vascular restricted and mesenchyme homeobox gene 2 (Meox2), a

key regulator of BBB functions showed a reduced expression (16%) in APOB-100 transgenic mice compared to WT animals (Figure 4). The gene expression of Mfsd2a, the BBB transporter for unsaturated lipid docosahexaenoic acid (DHA), was also decreased (44%; Figure 4). Lox-1, a lectin-like protein expressed in endothelial cells in the periphery is considered as the major receptor for oxidized low-density lipoprotein. The level Lox-1 gene expression increased dramatically (297%) in the microvessels of APOB-100 transgenic mice (Figure 4). Another protein family linked to the regulation of serum lipid concentrations is LDL receptor-related proteins (Lrps). While mRNA level of Lrp1 only slightly decreased (70%), the expression level of Lrp2 dropped to 56% in transgenic microvessels.

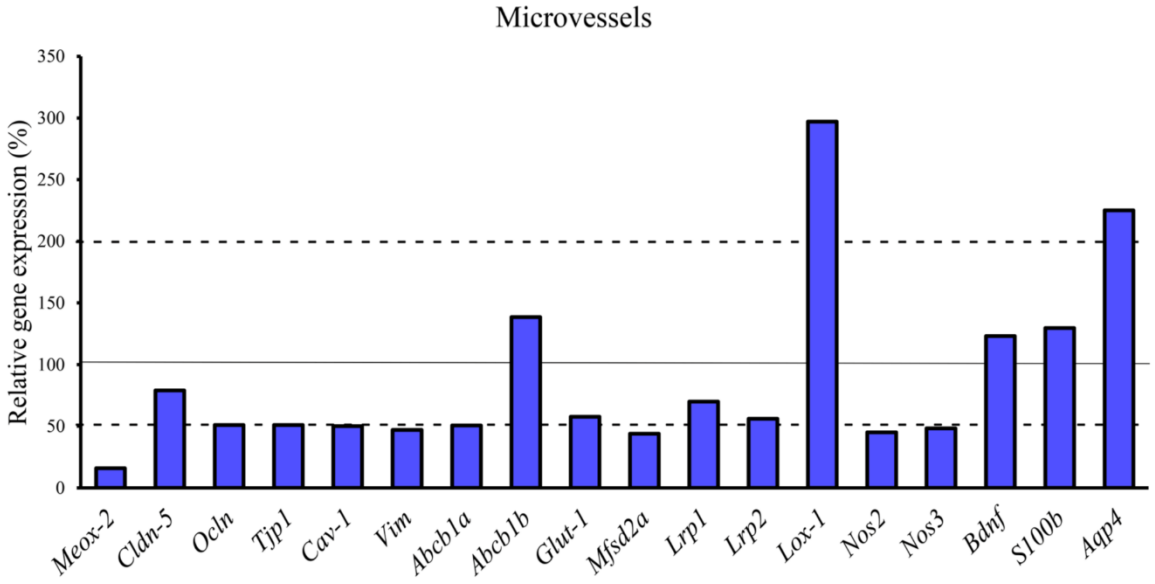

Figure 4. Gene expression analysis of the microvessel fraction from APOB-100 transgenic mice using qPCR. Continuous line indicates the expression level of the corresponding gene in WT mice (100%). Dashed lines indicate the levels of significant changes: a 2 fold (200%) increase or an 0.5 fold (50%) reduction in gene expression. $^{***}p<0.001$, $^{**}p<0.01$, $^{*}p<0.05$, compared with WT mice.

The gene expression of selected TJ proteins was also analyzed using qPCR. The mRNA level of transmembrane protein occludin, and TJ cytoplasmic linker ZO-1 (*Tjp-1*), was reduced to half in transgenic microvessels, while there was no change in the expression level of claudin-5, the dominant claudin member at the BBB, compared to WT animals. Further genes playing an essential role in BBB function, such as those of the primary glucose transporter in brain endothelial cells, Glut-1, and the efflux pump P-gp were also examined by qPCR in isolated brain microvessels. The gene expression level of Glut-1 dropped to 57%

in transgenic mice compared to WT animals. From the isoforms of P-gp coding genes, Abcb1a mRNA expression was significantly decreased (51%), while Abcb1b (138%) showed no significant change (Figure 4).

4.3.2. Expression levels of genes coding key cytokines involved in atherosclerotic processes

In order to study the molecular mechanisms leading from hypertriglyceridemia to BBB dysfunction expression levels of genes coding IL-6, a cytokine promoting atherosclerosis, and IL-10, a cytokine that may act as an IL-6 antagonist, were measured in isolated brain microvessels and in brain tissue using qPCR. IL-6 showed a significantly higher expression in cerebral microvessels compared to brain cortex in APOB-100 transgenic mice. IL-10 expression was under the detection limit in each sample (Figure 5).

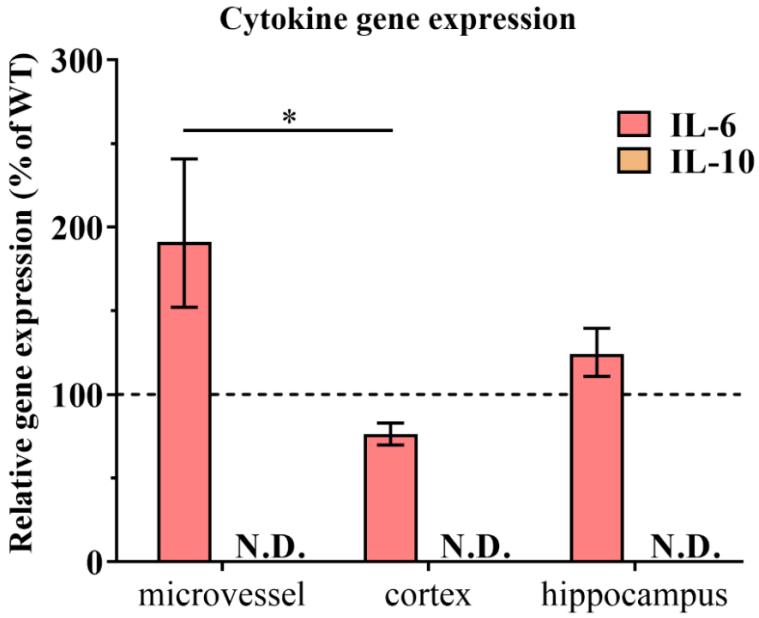

Figure 5. IL-6 and IL-10 gene expression levels measured with qPCR in isolated brain microvessels, cortex and hippocampus samples of WT and APOB-100 transgenic mice. IL-10 levels were under the detection limit.

4.4. Immunohistochemical staining pattern of key BBB proteins in the hippocampus and cortex of WT and APOB-100 transgenic mice

Taking into account that the increase in paracellular permeability might reflect expressional changes in TJ proteins, occludin and claudin-5 expression was examined at protein level, too. Fluorescence immunohistochemical staining showed that immunolabeling for occludin

and claudin-5 were exclusively localized at endothelial TJs and appeared as continuous lines (Figure 6). There was no statistically significant change neither in claudin-5 nor in occludin immunostaining intensity in transgenic cortex and hippocampus compared to WT animals (Figure 6).

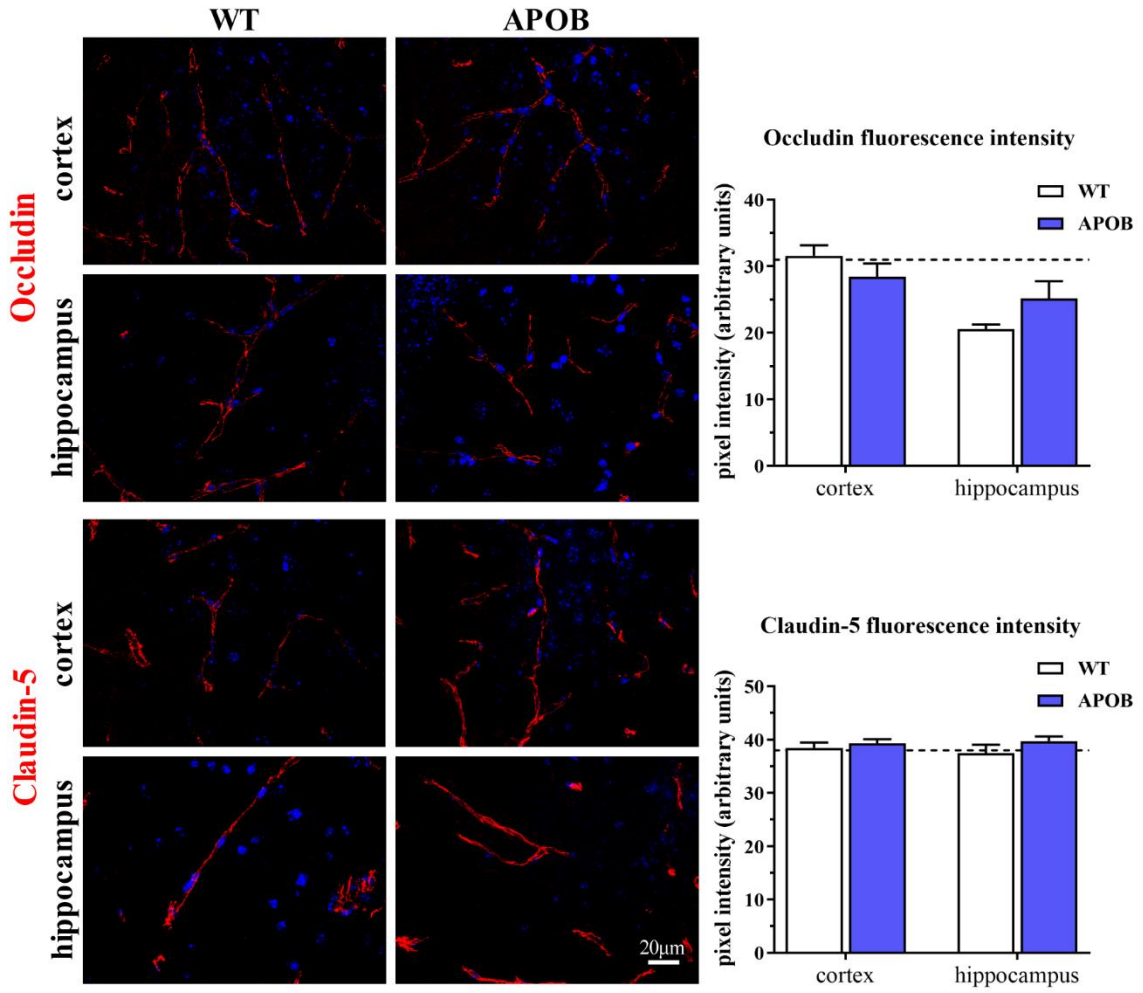

Figure 6. Immunostaining pattern of TJ proteins occludin and claudin-5 (both in red) in the cortex and hippocampus of WT and APOB-100 transgenic mice (APOB), counterstained with DAPI (blue), and quantification of the fluorescence intensities of occludin and claudin-5 immunolabeling in the frontal cortex and hippocampus of WT and APOB transgenic mice.

Another key BBB protein selected for immunohistochemical analysis was P-gp, based on the fact that one of the diagnostic features of the BBB in Alzheimer's disease is a decrease in P-gp expression, and APOB-100 transgenic mice are characterized by cognitive decline. Using a monoclonal antibody recognizing both isoforms of P-gp the immunoreactivity pattern of P-gp delineated a large number of capillaries in the frontal cortex and hippocampus in WT animals. However, in the APOB-100 transgenic group, P-gp immunoreactivity could hardly be observed in either brain region examined (Figure 7), which was reflected by a

significant drop in P-gp fluorescence intensity in APOB-100 transgenic mice compared to WT animals in the cortex and hippocampus, too (Figure 7).

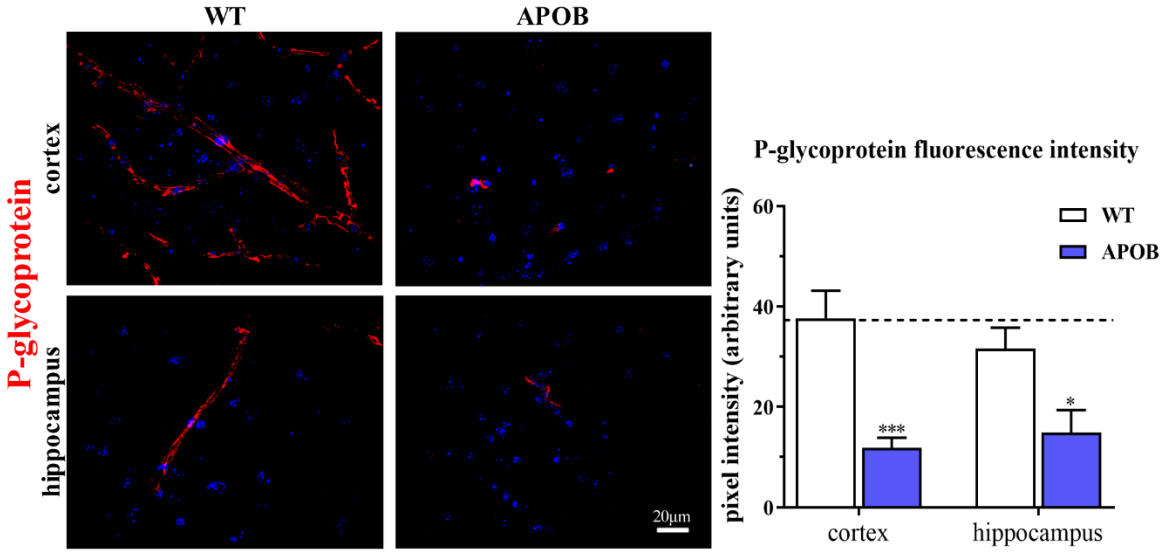

Figure 7. P-gp (ABCB1) transporter immunostaining pattern (red) in cortical and hippocampal areas of wild-type (WT) and APOB-100 transgenic mice (APOB), counterstained with DAPI (blue), and quantification of P-gp immunofluorescence intensity in the frontal cortex and hippocampus of WT and APOB transgenic mice. $^{***}p<0.001$, $^{*}p<0.05$, compared with WT mice.

4.5. Cell cultures

4.5.1. Cell viability studies

In our next series of experiments, we focused on actions of IL-6 and IL-10 exerted on brain endothelial cells, the major cell type of the BBB. Before studying IL-6 and IL-10 effects, the cell growth kinetics of brain endothelial cells from WT and APOB-100 animals was analyzed by impedance measurements on primary cultures of these cells. Based on the growth curves a slower proliferation rate in transgenic endothelial cell cultures was measured (Figure 8). Next, the effective concentration of cytokines on primary brain endothelial cell cultures was determined. IL-10 showed no harmful effects in either concentration, but IL-6 treatment resulted in a decrease in normalized cell index at a concentration of 50 ng/ml (Figure 8). At the higher concentration an early effect of IL-6 with steady decrease until 24 h was measured by impedance kinetics. This effect was antagonized by IL-10 when applied in combination with IL-6 (Figure 8).

The density of primary brain endothelial cell cultures was significantly decreased in transgenic cultures compared to WT cells under control conditions.

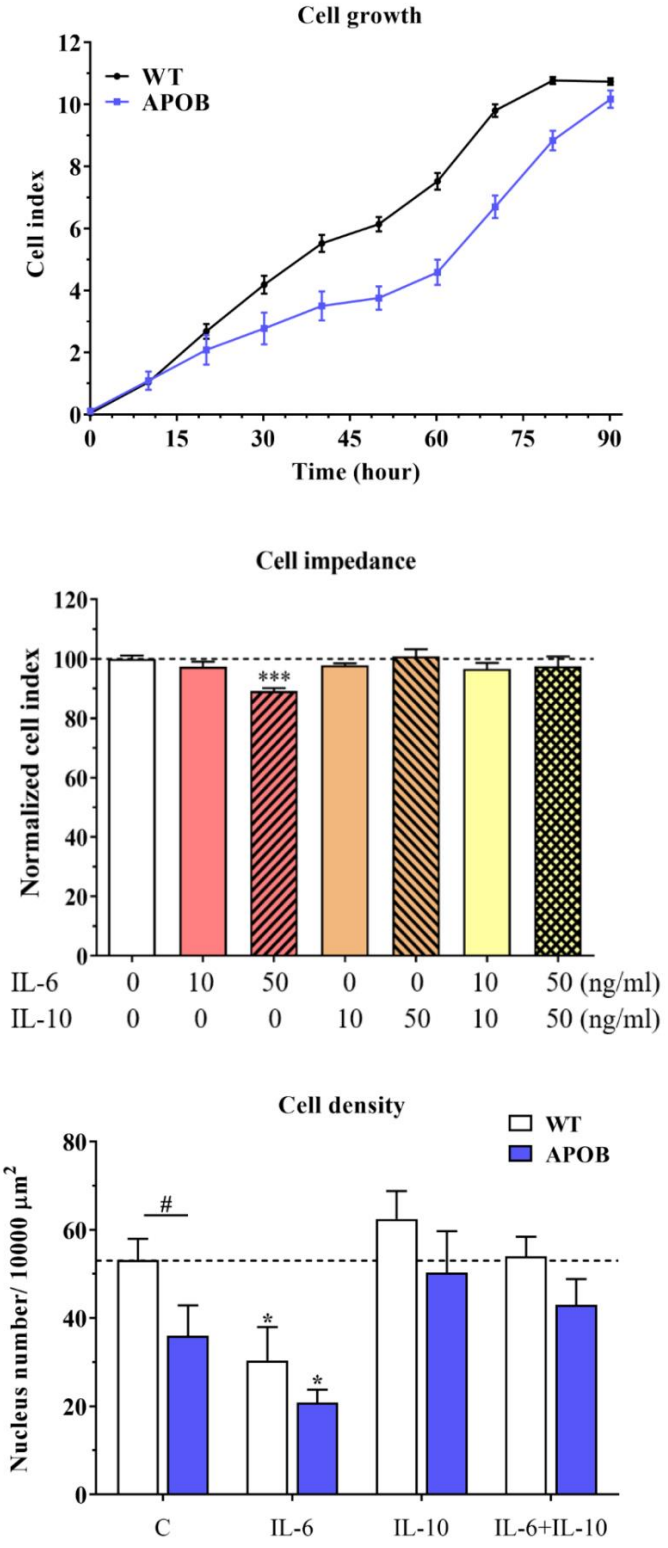

Figure 8. Cell viability assays on primary brain microvascular endothelial cells isolated from WT and APOB-100 transgenic mice: cell growth kinetics showing a slower growth in transgenic endothelial cell cultures, cell impedance measurements reflecting concentration dependent effects of IL-6, IL-10 and IL-6+IL-10 on WT endothelial cell viability, and changes in WT and APOB-100 endothelial cell density following IL-6, IL-10 and IL-6+IL-10 cytokine treatments at 50 ng/ ml concentration. * significant change due to cytokine treatment compared to the control group of the same genotype ($p<0.05$#: significant change between WT and APOB-100 cells ($p<0.05$).

Following treatment, the effective concentration of cytokines on primary brain endothelial cell cultures was determined. IL-10 showed no harmful effects in either concentration, but IL-6 treatment resulted in a decrease in normalized cell index at a concentration of 50 ng/ml (Figure 8). At the higher concentration an early effect of IL-6 with steady decrease until 24 h was measured by impedance kinetics. This effect was antagonized by IL-10 when applied in combination with IL-6 (Figure 8). The density of primary brain endothelial cell cultures was significantly lower in transgenic cultures compared to WT cells under control conditions. Following treatment of endothelial cell cultures with IL-6 (50 ng/ml) a significant decline in cell density was seen in both genotypes. However, when IL-6 was applied in combination with IL-10 no change was observed in cell density (Figure 8). Based on these results, both IL-6 and IL-10 were applied at a concentration of 50 ng/ml in all further experiments.

4.5.2. Brain endothelial cell function assays

Barrier integrity, a key brain endothelial cell function was monitored by TEER and permeability measurements and P-gp activity assays using co-culture BBB models. APOB-100 transgenic endothelial cells co-cultured with APOB-100 transgenic glial cells showed a decrease in TEER compared to the WT BBB co-culture model both with and without cytokine treatments. IL-6 resulted in more decreased TEER values in transgenic cells, which was not inhibited by IL-10. However, IL-10 applied alone did not change TEER compared to that measured in transgenic cells under control conditions. In WT cells, in contrast, a significant decrease in TEER was detected following each cytokine treatment compared to control values (Figure 9).

The permeability for the small molecular marker SF was increased in APOB-100 endothelial cells compared to WT cells in each experimental group. Following IL-6 treatment an increase in paracellular permeability was detected in WT cells and a further increase was observed in transgenic cells. IL-10 applied alone did not change permeability values in transgenic cells and did not antagonize IL-6 effects. Interestingly, IL-10 resulted in an increase in paracellular permeability in WT cells, which was not antagonized by IL-6 (Figure 9).

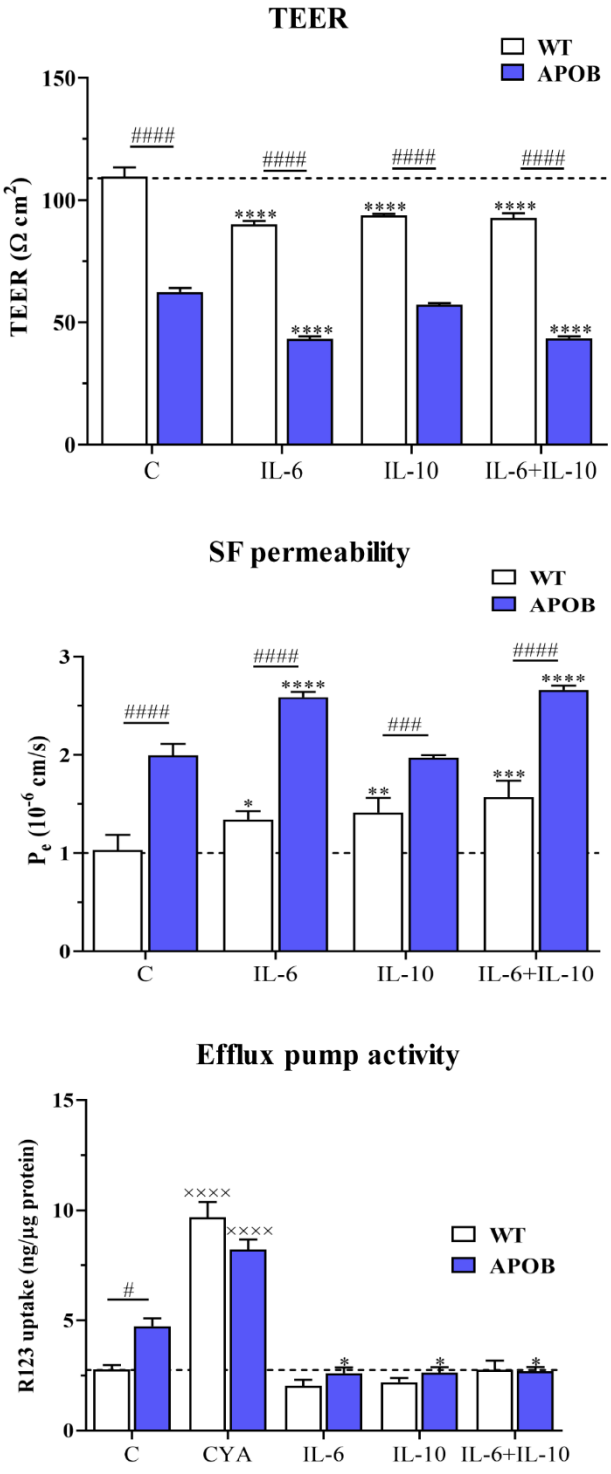

Figure 9. Effects of cytokine treatments on functional characteristics of brain microvascular endothelial cells: TEER values in WT and APOB-100 endothelial cell cultures treated with IL-6, IL-10, and their combination; permeability for sodium fluorescein (SF) in WT and APOB-100 endothelial cell cultures under control conditions and following cytokine treatments; activity of the efflux pump P-glycoprotein in WT and APOB-100 endothelial cell cultures. R123: rhodamine 123; CYA: cyclosporin A; $^{\#}$: significant change between WT and APOB-100 cells ($p<0.05$); * significant change due to cytokine treatment compared to the control group with the same genotype ($p<0.05$); ^{xxxx} significant change due to cyclosporin A ($p<0.0001$).

Another parameter which characterizes brain endothelial cell function is P-gp activity. A decreased P-gp activity, reflected in elevated cellular uptake of R123, was measured in brain endothelial cells isolated from APOB-100 transgenic mice compared to that detected in WT cells without cytokine treatment. This activity showed no change in WT cells following either cytokine application. Transgenic endothelial cells, in contrast, reacted to each cytokine applied with an increase in P-gp activity compared to activity levels seen in transgenic cells under basal conditions (Figure 9).

4.5.3. Analysis of endothelial cell morphology

In our next series of experiments morphological changes in WT and APOB-100 primary brain endothelial cell cultures were studied under control conditions and following cytokine treatments. The morphological analysis focused on immunostaining patterns of the efflux pump P-gp and of TJ proteins claudin-5, occludin and ZO-1.

P-gp immunolabeling was characterized by a patchy staining pattern in the cytoplasm of endothelial cells from both genotypes (Figure 10). The fluorescence intensity of P-gp immunolabeling showed a decrease in transgenic cells compared to WT cells under control conditions. The intensity of P-gp immunostaining was altered due to cytokine application. Brain endothelial cells isolated from WT mice showed a decrease in P-gp immunofluorescence after IL-6 treatment, resulting in intensity values similar to those measured in APOB cells under control conditions. This effect was antagonized by IL-10. No change in P-gp fluorescence intensity was observed in WT endothelial cells when IL-10 was applied alone. Transgenic cells exhibited a decrease in P-gp immunofluorescence intensity following treatment with the pro-inflammatory cytokine IL-6 and an increase in P-gp intensity after the anti-inflammatory cytokine IL-10 exposure, compared to control transgenic cells. IL-10 applied in combination with IL-6 antagonized the effects of IL-6 in both genotypes and resulted in immunofluorescence intensity values similar to those seen in control WT cells (Figure 10).

Regarding TJ proteins, claudin-5 and occludin immunostaining delineated endothelial cell borders as continuous lines in each experimental group (Figure 10). The intensity of claudin-5 immunofluorescence was similar in WT and APOB-100 transgenic endothelial cells under control conditions.

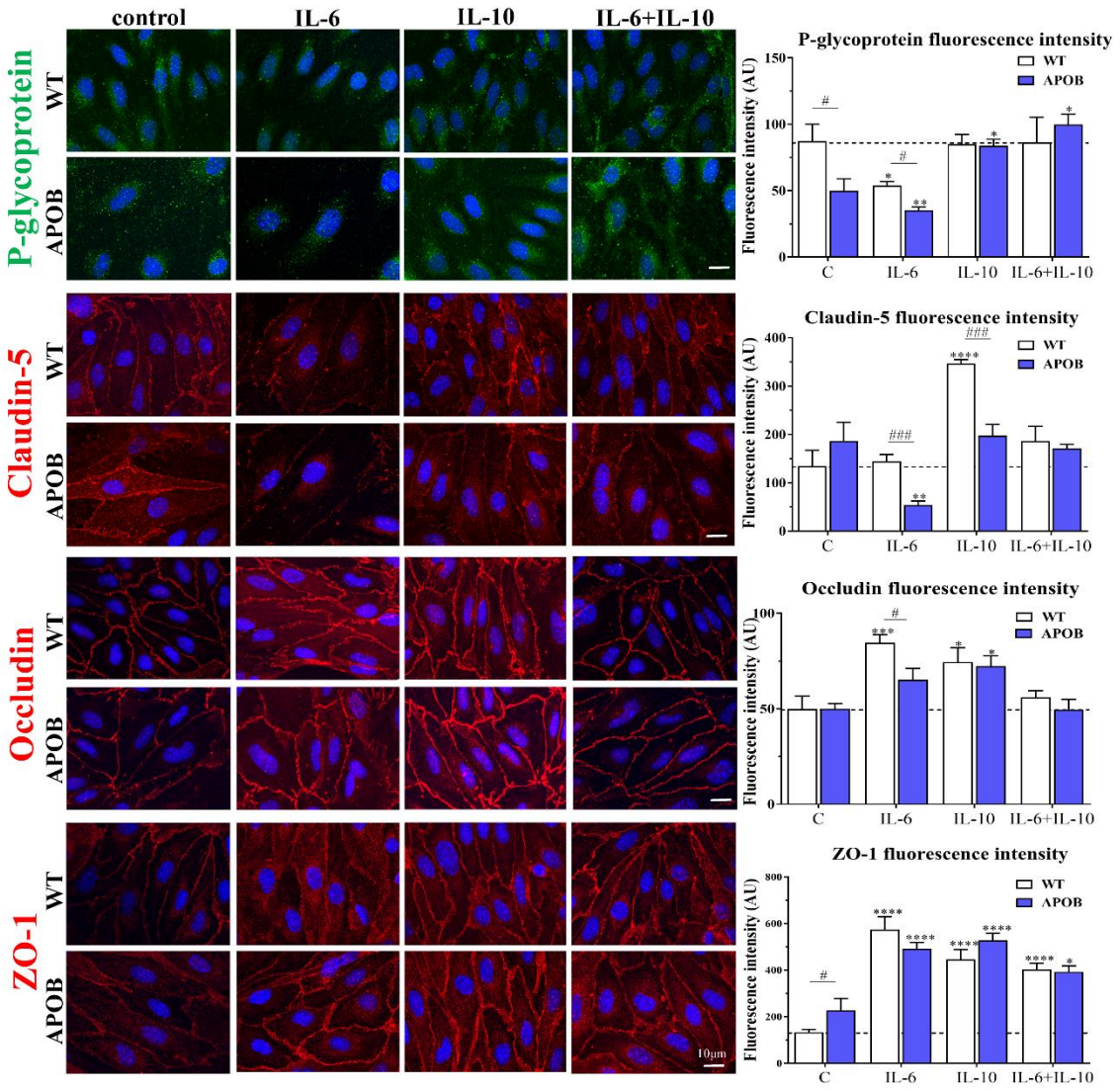

Figure 10. Immunostaining and fluorescence intensity of P-glycoprotein, claudin-5, occludin and zonula occludens protein-1 (ZO-1) in WT and APOB-100 brain endothelial cell cultures following cytokine treatments. AU: arbitrary unit; #: significant change between WT and APOB-100 cells ($p<0.05$); * significant change due to cytokine treatment compared to the control group with the same genotype ($p<0.05$).

A dramatic decrease in claudin-5 immunofluorescence intensity was observed following IL-6 in transgenic cells compared to control cells. This change was prevented by combining IL-6 with IL-10. Endothelial cells from WT mice showed no change in claudin-5 intensity after IL-6 exposure, but a significant increase in fluorescence intensity was detected following IL-10 treatment (Figure 10). The intensity of occludin immunofluorescence was similar in endothelial cells from both genotypes under control conditions. An increased fluorescence intensity was measured in WT cells following IL-6 and IL-10 treatments, but this effect was not detected after applying IL-6 and IL-10 in combination. APOB-100 endothelial cells showed an increase in occludin immunofluorescence after IL-10 exposure.

No change in occludin fluorescence intensity was observed following other cytokine treatments (Figure 10). ZO-1 immunolabeling was present characteristically not only in cell borders but in the cytoplasm too, under control conditions especially in transgenic cells. Following each cytokine treatment, the cytoplasmic localization of ZO-1 was abundant in both genotypes. The intensity of ZO-1 immunofluorescence labeling was higher in transgenic cells under basal conditions. A significant increase in immunofluorescence intensity was seen in both genotypes after cytokine application (Figure 10).

4.5.4. Cytokine effects on cultured glial cells

In our next series of experiments other cellular components of the neurovascular unit, namely astro- and microglial cells were studied *in vitro*. Mixed astro/microglia cultures are suitable tools to study changes in astro- and microglia density and in the ratio of astro/microglial cells, which may reproduce glial reactions occurring *in vivo*.

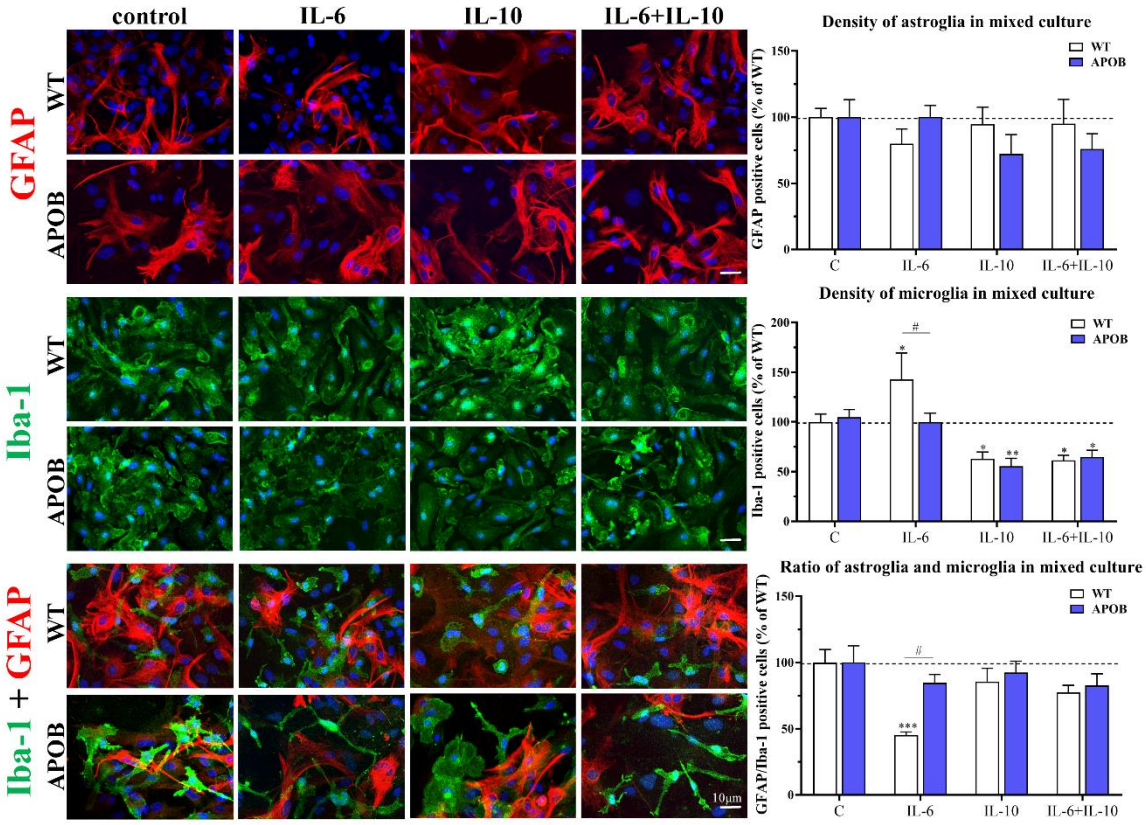

Figure 11. Changes in in primary glial cell cultures isolated from WT and APOB-100 transgenic mice following IL-6, IL-10 and IL-6+IL-10 cytokine treatments. Astroglia cells were immunostained for **GFAP**, microglia cells were immunostained for **Iba-1**. #: significant change between WT and APOB-100 cells ($p<0.05$); * significant change due to cytokine treatment compared to the control group with the same genotype ($p<0.05$).

Astrocytes showed similar densities under control conditions and in all cytokine treated groups in both genotypes (Figure 11). The density of microglial cells without cytokine treatment was also similar comparing the two genotypes. Following IL-6 treatment WT microglia showed an increase in density. In contrast, after IL-10 exposure, applied either alone or in combination with IL-6, a decreased microglia density was observed in both genotypes, compared to their respective controls (Figure 11). The astro/microglia ratio under control conditions was also similar in APOB-100 transgenic and WT mixed glial cell cultures. In APOB-100 glial cell cultures no change in astro/microglia ratio was measured following either cytokine treatment. In contrast, in WT cultures a significant decrease in astro/microglia ratio was observed following IL-6 treatment. This effect was not seen when IL-6 and IL-10 were applied in combination. IL-10 alone did not have any effect on astro/microglia ratio in WT glial cells (Figure 11).

The characteristic protein of astroglial endfeet, the water channel AQP4, was examined in cultured astrocytes isolated from WT and APOB-100 mice (Figure 12).

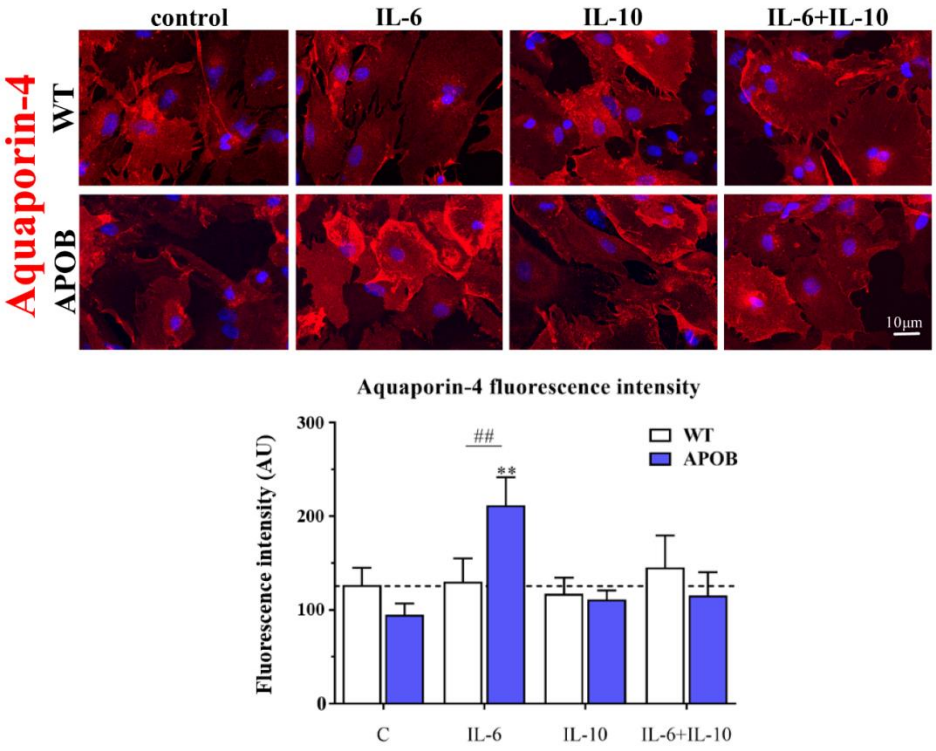

Figure 12. Changes in aquaporin-4 immunostaining pattern and fluorescence intensity in cultured astroglial cells. The cells were isolated from WT and APOB-100 transgenic mice and treated with IL-6, IL-10 and IL-6+IL-10 cytokines, respectively. AU: arbitrary unit. #: significant change between WT and APOB-100 cells ($p<0.05$); * significant change due to cytokine treatment compared to the control group with the same genotype ($p<0.05$).

The specificity of AQP4 immunolabeling was confirmed by its colocalization with the astroglia marker S100b. AQP4 immunofluorescence intensity was similar in primary astroglia cultures comparing the two genotypes under basal conditions. A significant increase in the intensity of AQP4 immunofluorescence was observed in APOB-100 transgenic astrocytes following IL-6 exposure. This effect was not seen when IL-6 was applied in combination with IL-10. No change in AQP4 fluorescence intensity was detected in transgenic astroglia when they were treated with IL-10 alone. AQP4 immunofluorescence intensity showed no change in primary astroglia cultures isolated from WT mice after either cytokine treatment (Figure 12).

4.6. Morphological study of brain microvessels

Morphological analysis of P-gp and TJ proteins expressed by endothelial cells and of AQP4 localized mainly in astroglial endfeet was carried out in isolated brain microvessels (Figure 13). The immunostaining of the efflux pump P-gp in isolated microvessels displayed an inhomogeneous pattern with dense patches in parts in the WT control group. In microvessels isolated from APOB-100 transgenic mice and in all cytokine treated WT microvessels the P-gp immunoreactivity pattern showed a more uneven appearance. The area fraction of P-gp labeling was significantly higher in WT microvessels compared to transgenics under basal conditions (Figure 13). Microvessels isolated from APOB-100 transgenic mice showed no change in the pattern of P-gp immunostaining following cytokine treatments. In contrast, a decrease in P-gp immunolabeled area fraction was observed in WT microvessels after each cytokine exposure (Figure 13). Claudin-5 and occludin immunostained area fractions were similar in WT and APOB-100 transgenic microvessels without cytokine treatment. No change in these immunostained area fractions was detected after cytokine exposures (Figure 13). ZO-1 immunostaining, like other TJ proteins, showed no significant difference in immunolabeled area fraction in microvessels isolated from WT and APOB-100 transgenic animals. Transgenic microvessels were not responsive to cytokine treatments. In contrast, a decrease in immunolabeled area fraction was measured in WT microvessel after each cytokine application (Figure 13). The immunolabeling of the astrocyte endfeet marker AQP4 was characterized by a similar area fraction in WT and APOB-100 microvessels without cytokine treatment. Application of the pro-inflammatory cytokine IL-6 resulted in a decrease in AQP4 immunostained area fraction compared to controls in WT microvessels. This effect was antagonized by IL-10 in WT microvessels,

while IL-10 applied alone had no effect on AQP4 area fraction. In transgenic microvessels, in contrast, AQP4 area fraction did not change after IL-6 or IL-10 exposure, but showed a decrease when IL-6 was applied in combination with IL-10, and no antagonistic effect was observed (Figure 13).

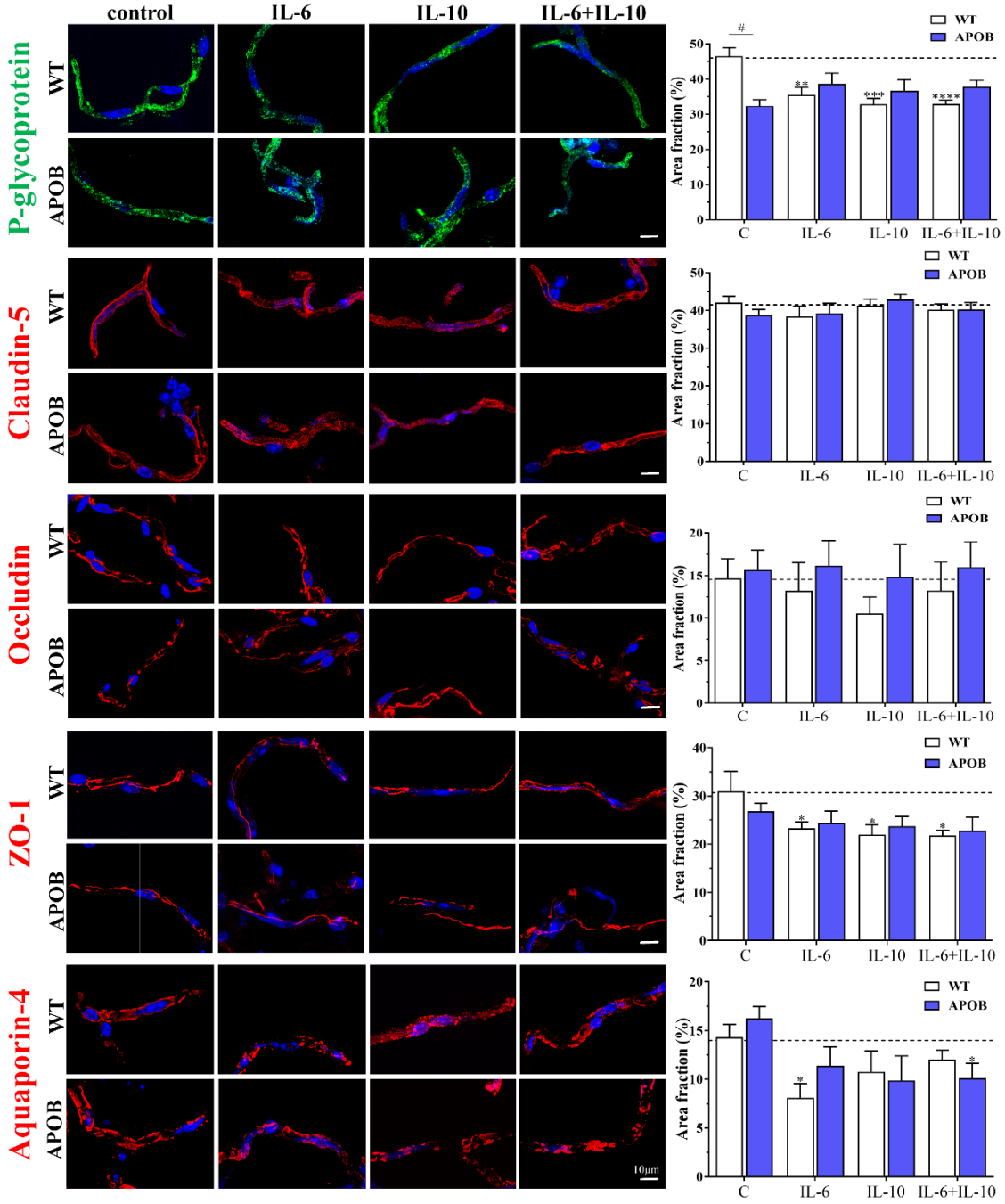

Figure 13. Changes of endothelial and astroglial cell markers in isolated brain microvessels. Microvessels were isolated from WT and APOB-100 transgenic mice, treated with IL-6, IL-10 and IL-6+IL-10 cytokines and immunostained for P-glycoprotein, claudin-5, occludin, zonula occludens protein-1 (ZO-1) and aquaporin-4. #: significant change between WT and APOB-100 cells ($p<0.05$); * significant change due to cytokine treatment compared to the control group with the same genotype ($p<0.05$).

5. Discussion

5.1. *In vivo* experiments

Transgenic mice overexpressing the human APOB-100 protein show chronic hypertriglyceridemia, an increase in permeability for a small molecular marker, and gene expressional, immunohistochemical and ultrastructural alterations at the BBB.

Lipolysis products generated from triglyceride rich lipoproteins damage endothelial barrier function: perturb the expression of junctional proteins, induce apoptotic cell death *in vitro* in human aortic endothelial cells (Eiselein et al., 2007) and transiently elevate BBB permeability *in vivo* in mice (Lee et al., 2017). Hypertriglyceridemia may contribute to endothelial dysfunction likely through the generation of oxidative stress (Antonios et al., 2008). Indeed, our research group has shown that oxidized LDL treatment induced barrier dysfunction and increased reactive oxygen species production and membrane rigidity in primary brain endothelial cells (Lénárt et al., 2015).

Our present findings are in accordance with earlier data indicating that APOB-100 transgenic mice are characterized by chronic hypertriglyceridemia (Süle et al., 2009). Regarding BBB function, a significantly increased extravasation for a small molecule marker, SF, was observed in the hippocampus of transgenic mice. This may suggest an increase in paracellular permeability of brain endothelial cell layers. The BBB dysfunction detected in our model may be linked to reduced expression of genes coding important brain endothelial TJ proteins occludin, claudin-5, Tjp-1. However, the differences detected at mRNA level were not reflected by the immunostaining pattern of TJ proteins occludin and claudin-5, suggesting no detectable changes of TJs between the experimental groups using conventional confocal microscopy.

Several genes playing a role in regulating BBB functions, including the homeobox regulator Meox2 and BBB transporters Mfsd2a, Glut1, Lrp2, Abcb1a, showed a reduced expression in APOB-100 transgenic animals. It suggests brain endothelial dysfunction in our model and may indicate pathomechanisms similar to those observed in other conditions of BBB damage (Zlokovic, 2011; Zhao et al., 2015). Our observations on the drastically reduced Meox2 in transgenic brain microvessels might also support the link between Meox2 and neurovascular dysfunction. Beside Meox2 the other gene for which a dramatic decrease was observed in brain microvessels from transgenic animals was Mfsd2a, which might have contributed to the increased BBB permeability in our study and the neurodegeneration in our model

described previously (Bereczki et al., 2008). Mfsd2a is reported to act not only as a docoshexaenoic acid transporter at the BBB, but also as a key regulator of BBB integrity and function (Zhao and Zlokovic, 2014).

At the BBB GLUT1 is the main transporter of glucose, the primary energy source in the brain. A reduction in Glut1 expression was linked to neurovascular dysfunction in a mouse model (Winkler et al., 2015) emphasizing the importance of the present findings.

Additionally, the genes coding receptors Lrp1, Lrp2 and especially the Abcb1a gene coding the P-gp isoform predominantly expressed in brain capillary endothelial cells (Croop et al., 1989; Shoshani et al., 1998) showed a decreased expression in microvessels isolated from APOB-100 transgenic mice. These receptors and the efflux pump P-gp are responsible for the clearance of amyloid β from the brain (Shibata et al., 2000; Deane et al., 2003; Cirrito et al., 2005). Their reduced expression is likely to contribute to the accumulation of amyloid β plaques, which was observed earlier in this transgenic mouse strain (Bereczki et al., 2008). In agreement with this finding, we could hardly detect any P-gp immunolabeling in APOB-100 transgenic mouse brains.

5.2. *In vitro* and *ex vivo* experiments

The functional and morphological changes of the BBB observed in APOB-100 transgenic mice are likely related to hypertriglyceridemia, which is closely linked to cardio-and cerebrovascular pathologies. We hypothesized that the pleiotropic pro-inflammatory cytokine IL-6, a key regulatory element in atherosclerotic processes, may significantly contribute to BBB dysfunction. To test this hypothesis, the effects of IL-6 and IL-10, an antagonist of IL-6, were examined on brain endothelial and glial cell cultures, and on isolated brain microvessels.

5.2.1. Primary brain microvascular endothelial cell cultures

5.2.1.1. Functional characteristics

Under basal, unstimulated culture conditions APOB-100 brain endothelial cells grew slower than WT cells. It was also reflected in lower endothelial cell density in the transgenic group. This difference in cell growth may, at least in part, be a consequence of the expression of the APOB-100 transgene in cultured brain endothelial cells, as we demonstrated previously (Lénárt et al., 2015), and the proinflammatory microenvironment of the cerebral microvessels from which endothelial cells were isolated (Tóth ME et al., 2020; Hoyk et al., 2018). This is in line with the present finding that IL-6 gene expression was significantly

higher in microvessels than in brain tissue in APOB-100 transgenic animals. Thus, cultured APOB-100 brain endothelial cells could be primed with IL-6 without further cytokine treatments. IL-10 applied alone did not influence either cell viability or cell density, but it antagonized IL-6 effects on both parameters when applied in combination with IL-6 (Figure 14). This is in concordance with data showing that IL-10 downregulates inflammatory genes and antagonizes IL-6 actions (Dinarello, 2007; Murray, 2005).

As compared to the WT, the APOB-100 BBB model showed a paracellular barrier dysfunction based on the decreased TEER values and enhanced permeability for SF under control conditions (Figure 14). We measured increased BBB permeability in APOB-100 transgenic animals earlier (Hoyk et al., 2018), which supports the present observation. IL-6 is known to induce a dose- and time-dependent decrease in TEER in rat brain endothelial cell monocultures (de Vries et al., 1996). In accordance with this, IL-6 decreased TEER and increased paracellular permeability in both WT and APOB-100 BBB co-culture models in our present experiments (Figure 14). Effects of IL-10 on *in vitro* BBB function were examined for the first time in our present experiments. We observed a decrease in TEER and an increase in SF permeability in the WT BBB co-culture model. APOB-100 transgenic brain endothelial cells, which are characterized by weaker paracellular barrier properties in control conditions, showed no change in these parameters following IL-10 treatment. The alterations in TEER and SF permeability seen after IL-6 application were not antagonized by IL-10 in either genotype (Figure 14). Our data may result from a difference in cytokine expression in the WT compared to the APOB-100 brain. APOB-100 brain endothelial cells are isolated from an inflamed condition. Consequently, these cells are sensitive to treatment with the pro-inflammatory cytokine IL-6, but the anti-inflammatory IL-10 exposure is not harmful for them. In contrast, exposing WT brain endothelial cells either to IL-6 or IL-10 may result in an imbalance in their microenvironment, leading to decreased TEER and increased permeability values.

Our present results show that P-gp activity, another feature of BBB function, decreased in APOB-100 brain endothelial cells compared to WT cells without cytokine treatment (Figure 14). Data on P-gp activity measured *in vivo* in neuroinflammatory conditions are reported in relation to neuroinflammatory and neurodegenerative diseases. P-gp is overexpressed in epilepsy (Feldmann et al., 2013) and amyotrophic lateral sclerosis (Mohamed et al., 2017), and downregulated in Parkinson's and Alzheimer's diseases, where it leads to impaired β-amyloid clearance (Sweeney et al., 2018). Under basal conditions P-gp

activity in APOB-100 brain endothelial cells was reduced similarly to results observed in Parkinson's or Alzheimer's diseases. Both IL-6 and IL-10 treatments resulted in an improved P-gp activity compared to control conditions in the transgenic cells, while the efflux pump activity did not change in WT brain endothelial cells (Figure 14). The published findings related to IL-6 effects on P-gp function are contradictory. IL-6 reduced P-gp function in cultured guinea pig brain endothelial cells (Iqbal et al., 2012), while it did not change P-gp activity in a human BBB model (Poller et al., 2010). IL-6 is involved in the pathogenesis of amyotrophic lateral sclerosis (Ono et al., 2001; Ehrhart et al., 2015), a pathologic condition where P-gp activity is increased (Mohamed et al., 2017). The elevated P-gp activity in APOB-100 brain endothelial cells treated with IL-6 may reflect an increased cellular vulnerability. Regarding IL-10 action, the observed improvement of P-gp function in transgenic brain endothelial cells may indicate a compensatory mechanism against some inflammatory processes (Dinarello, 2007) going on in hypertriglyceridemic mice from which endothelial cells were derived. WT endothelial cells, in contrast, showed a more stable P-gp activity, which was not altered by either cytokine treatment at least in the concentrations applied. The decreased P-gp activity detected in cultured APOB-100 brain endothelial cells compared to WT cells was paralleled by a decrease in P-gp immunofluorescence intensity under basal conditions. These changes are in line with our earlier results showing a decrease in P-gp immunofluorescence intensity of microvessels in brain sections of APOB-100 transgenic mice (Hoyk et al., 2018). The P-gp immunostaining pattern in our primary mouse brain microvessel endothelial cell cultures was similar to that seen in our previous works on rat (Nakagawa et al., 2009; Hellinger et al., 2012) and earlier publications on rat and bovine BBB models (Greenwood, 1992; Helms et al., 2014). Regarding IL-6 effects on P-gp protein expression, the published results tend to show a reduction in P-gp content after pro-inflammatory cytokine treatments (Fernandez et al., 2004; Sukhai et al., 2001), which supports our present data (Figure 14). IL-10, in contrast, resulted in an increase in P-gp immunofluorescence intensity in APOB-100 endothelial cells and antagonized IL-6 effects both in WT and APOB-100 brain endothelial cells. These data provide further support for the antagonistic actions of IL-6 and IL-10, and demonstrate for the first time that P-gp expression in brain microvascular endothelial cells may be enhanced by IL-10.

5.2.1.2. Morphological characteristics

The major proteins determining TEER and paracellular permeability at the BBB are TJ proteins. An immunocytochemical analysis of TJ proteins in microvessel endothelial cells isolated from WT and APOB-100 transgenic mouse brains under basal conditions was described in our earlier publication (Lénárt et al., 2015). In that study cytoplasmic linker ZO-1 showed a significant increase in fluorescence intensity in APOB-100 endothelial cells compared to WT cells, but no difference was found in integral membrane TJ proteins claudin-5 and occludin fluorescence intensity. Our present results partly confirm these earlier findings and provide new data on TJ protein expressional changes following IL-6 and IL-10 treatments. Among TJ proteins claudins are fundamental elements in the regulation of paracellular permeability and their expression is reduced due to inflammation (Günzel and Yu, 2013). The pro-inflammatory cytokine IL-6 reduced claudin-5 expression in human and in rat brain microvascular endothelial cell cultures (Rochfort et al., 2014; Camire et al., 2015). In our murine brain microvascular endothelial cell cultures, a decrease in claudin-5 fluorescence intensity was detected in APOB-100 transgenic cells after IL-6 treatment, which was prevented by a simultaneous IL-10 application (Figure 14). This observation is supported by data indicating that IL-10 attenuated the decrease in claudin-5 expression induced by the pro-inflammatory cytokine TNF-α in rat brain endothelial cell cultures (Camire et al., 2015). Furthermore, IL-10 attenuated the increase in BBB permeability and the downregulation of claudin-5 in a rat model of severe acute pancreatitis (Lin et al., 2018). WT brain endothelial cells, in contrast, showed no change in claudin-5 fluorescence intensity after IL-6 treatment. This suggests a possible difference in sensitivity to pro-inflammatory cytokines of brain endothelial cells in different species and strains within species. An increased sensitivity to IL-6 in APOB-100 transgenic compared to WT cells can also be concluded (Figure 14). Following IL-10 exposure an increase in claudin-5 immunostaining intensity measured in all cell areas including the cytoplasm was observed in WT brain endothelial cell cultures. This is in line with our results showing a decrease in TEER and an increase in paracellular permeability in WT endothelial cells treated with IL-10, indicating that a balanced cytokine microenvironment is needed for optimal claudin-5 expression, localization and BBB function.

Occludin fluorescence intensity showed similar values in WT and APOB-100 endothelial cells without cytokine treatment (Figure 14), which confirmed our earlier results (Lénárt et al., 2015). An increase in the intensity of occludin immunofluorescence was detected in WT

brain endothelial cells after IL-6 and IL-10 treatments and in APOB-100 brain endothelial cells following IL-10 application. Occludin is reported to undergo a continuous endocytosis from the plasma membrane into the cytoplasm, followed by a recycling back to the plasma membrane (Fletcher et al., 2014). A possible regulatory mechanism of occludin turnover involves glycogen synthase kinase 3β (GSK3β), an ubiquitously expressed serine/threonine kinase having multiple functions. GSK3β was downregulated in IL-6 treated hepatocytes (Wigmore et al., 2007). Inhibition of GSK3β resulted in increased occludin levels in brain endothelial cells based on western blot studies (Ramirez et al., 2013). This is a possible mechanism that may explain the increase in occludin fluorescence measured in WT endothelial cells after IL-6 exposure, while the GSK3β in APOB-100 endothelial cells may be less sensitive to IL-6. On the other hand, occludin endocytosis may be enhanced by IL-10, since IL-10 is capable of inducing actin filament rearrangements leading to endocytosis (Lucero et al., 2020). IL-10 may promote endocytosis in both WT and APOB-100 endothelial cells, contributing to occludin internalization, which may result in an increase in occludin immunofluorescence intensity. Furthermore, a recent study found that occludin increase may compensate for a loss in claudin-5 at the BBB in claudin-5 null mouse embryo (Sasson et al., 2021).

Another TJ protein examined in the present study is ZO-1, which participates in actomyosin organization, cell-cell tension, cell migration, angiogenesis and barrier formation in endothelial cells (Tornavaca et al., 2015). In our models an increase in ZO-1 immunofluorescence intensity was observed in APOB-100 transgenic endothelial cells compared to WT cells under control conditions and in both genotypes following all cytokine treatments (Figure 14) most possibly due to changes in ZO-1 intracellular distribution. Our observations are supported by findings that report a decrease in ZO-1 mRNA levels and a redistribution of ZO-1 protein from the cell borders toward cellular nuclei after IL-6 application in human brain microvascular endothelial cell cultures (Rochfort et al., 2015). ZO-1 relocalization was also seen in brain endothelial cells in a mouse model of multiple sclerosis (Bennett et al., 2010). IL-10 exerted similar effects as IL-6 on changes in ZO-1 immunofluorescence intensity.

5.2.2. Glial cell cultures

Our *in vitro* experiments focused not only on endothelial cells, but on glial components of the neurovascular unit, too. First, changes in cell density of cultured astro- and microglia were analyzed to examine whether IL-6 applied at the concentration of 50 ng/ml in

endothelial cell cultures was also effective in our glial cell cultures. The observed increase in WT microglia density served as a proof of effectiveness of the IL-6 concentration in cultured glial cells (Figure 14). It suggests an increase in microglia proliferation after IL-6 application, which is in line with data describing similar IL-6 effects (Streit et al., 2000). The lack of reactivity to IL-6 treatment in APOB-100 transgenic microglia may result from a decreased sensitivity to IL-6, since these cells are derived from chronic neuroinflammatory conditions. Chronic exposure to IL-6 is reported to induce a desensitized microglia phenotype (Recasens et al., 2021). IL-10, in contrast, is known to reduce microglia proliferation (Kloss et al., 1997; Recasens et al., 2019), which confirms our present results seen both in WT and APOB-100 glial cell cultures. Our data suggest that IL-10 antagonizes IL-6 effects on density in both WT and APOB-100 microglia cells. Regarding astrocytes, in our present experiments no significant changes were detected in astroglia density at 24 h following cytokine treatments. There are conflicting data on IL-6 effects on astroglia proliferation rate (Benveniste et al., 1989; Selmaj et al., 1990), while IL-10 is unanimously reported to promote proliferation of astroglia (Hersh et al., 2021). The lack of reactivity to cytokine treatments in our cultured astrocytes at 24 h indicates that astroglia proliferate in response to stimuli later then microglia, similarly to reactions going on *in vivo*. The changes occurring in parallel in micro- and astroglial cells in our mixed cultures resulted in a significant decrease in the astro-/microglia ratio in WT glial cultures following IL-6 treatment which was antagonized by IL-10 (Figure 14).

The water channel AQP4, a marker protein of astroglial endfeet, was analyzed in WT and APOB-100 astroglia cultures. AQP4 upregulation is reported during neuroinflammation (Sugimoto et al., 2015) and IL-6 is a known driving force in this process (Sun et al., 2017). Our present results showing an increase in AQP4 fluorescence intensity following IL-6 treatment in cultured APOB-100 astrocytes (Figure 14) are in accordance with these data, and demonstrate that IL-6 effects on AQP4 expression in APOB-100 astrocytes may be dependent on the inflammatory microenvironment. No change in AQP4 fluorescence intensity was seen in the WT group following IL-6. The anti-inflammatory cytokine IL-10 antagonized IL-6 actions on AQP4 fluorescence intensity changes in APOB-100 astroglial cells.

5.2.3. *Ex vivo* experiments – isolated brain microvessels

We examined cytokine effects on immunostaining patterns of key proteins playing a role in BBB function not only in cell cultures, but also in isolated brain microvessels. This *ex vivo*

system has more similarity to *in vivo* conditions, since in these isolated microvessels brain endothelial cells are surrounded by pericytes (Veszelka et al., 2007) and astrocytic endfeet. Consequently, cellular interactions may modulate the effects of cytokine treatments. To preserve the *ex vivo* function of isolated brain microvessels, cytokine treatments lasted for one hour, in contrast to the one-day treatment length of cell cultures.

P-gp immunolabeling in isolated brain microvessels showed a reduction in the transgenic group compared to WT brain microvessels under control conditions as described in our earlier publication using brain sections (Hoyk et al., 2018). This decreased P-gp staining was also observed in primary brain endothelial cell cultures, as shown in Figure 14. The reactivity to cytokines, however, was different in microvessels compared to brain endothelial cell monocultures. In APOB-100 microvessels, characterized by a reduced P-gp immunolabeling, no further decrease to cytokine treatments was seen. This lack of reactivity to IL-6 and IL-10 application may result from the increased IL-6 production in APOB-100 microvessels under basal conditions, as it was observed in our qPCR experiments (Figure 5). WT microvessels, in contrast, showed a decrease in area fraction of P-gp immunolabeled structures in each cytokine treated group. It resulted in a P-gp immunolabeling pattern similar to that seen in transgenic microvessels (Figure 13). Astrocytic endfeet and pericytes, which are present in isolated microvessels around endothelial cells, are known to regulate endothelial cell polarity, function and P-gp localization (Wolburg-Buchholz et al., 2009; Al Ahmad et al., 2011). Moreover, both astrocytes and pericytes are capable to secrete IL-6 and IL-10 (Kovac et al., 2011), and astrocytes themselves are responsive to both IL-6 and IL-10 (Aniszewska et al., 2015; Ledeboer et al., 2002). The possibility of a complex cellular interaction and reactivity to cytokines in isolated microvessels may explain the differences detected in P-gp immunolabeling in isolated microvessels compared to brain endothelial cell monocultures.

In contrast to brain endothelial cell monocultures, isolated brain microvessels showed no change in claudin-5 and occludin immunostaining after 1-hour cytokine exposures (Figure 14). IL-6 is reported to induce a decrease in claudin-5 and occludin protein expression in microvessels from adult sheep at a concentration of 100 ng/ml, but no change was detected in these protein levels when IL-6 was applied at 10 ng/ml (Cohen et al., 2013). This indicates that IL-6 effects on claudin-5 and occludin expression are dose dependent in microvessels. In the present paper we used IL-6 at a concentration of 50 ng/ml, which might not be a concentration high enough to affect claudin-5 and occludin expression.

ZO-1, another TJ protein analyzed in our experiments, showed a decrease in immunolabeled area fraction in WT microvessels following each cytokine treatment (Figure 14). In a previous study we also demonstrated a reduced ZO-1 immunolabeling in isolated rat brain microvessels in inflammatory condition (Veszelka et al., 2007). ZO-1 immunoreactive area fraction in APOB-100 microvessels, in contrast to the WT, remained the same after each cytokine treatment as in control conditions. A similar decrease in sensitivity to IL-6 and IL-10 application was detected in P-gp immunoreactive area fraction in the transgenic microvessels, suggesting that P-gp and ZO-1 immunoreactivity may share some regulatory features. The differences seen in ZO-1 changes in brain endothelial cells in culture and in isolated microvessels may partly be due to differences in cytokine treatment times in the two systems.

In addition to TJ proteins characteristic to cerebral endothelial cells, the immunostaining pattern of AQP4, a specific component of astrocytic endfeet, was also analyzed in isolated brain microvessels. Under basal conditions no difference was seen between AQP4 area fractions measured in WT and APOB-100 microvessels. However, the sensitivity to cytokine treatments was different comparing the two genotypes. WT microvessels reacted to IL-6 treatment only, while microvessels isolated from transgenic mice showed a decrease in AQP4 immunolabeled area fraction following a combined IL-6 + IL-10 exposure. Decreases in the AQP4 immunolabeled area fractions in isolated brain microvessels may suggest either reductions in AQP4 protein expression or relocalization of the AQP4 protein in astrocytic endfeet. Our previous study analyzing brain capillary ultrastructure in APOB-100 transgenic mice indicated edema of astroglia endfeet, which was in line with an increased expression of the AQP4 gene in isolated microvessels (Hoyk et al., 2018). Therefore, we hypothesize that the observed decreases in AQP4 area fractions are the consequences of a disturbance in the normal localization of the water channel AQP4. Mislocalization of AQP4 was reported in epilepsy and a loss of AQP4 in astroglial endfeet was found in mouse models of Alzheimer's disease and multiple sclerosis indicating BBB impairment (Wolburg-Buchholz et al., 2009; Hubbard et al., 2018; Yang et al., 2011). In isolated brain microvessels the principal cellular targets of IL-6 and IL-10 are endothelial cells and/or pericytes, which can, in turn, affect AQP4 localization in astroglial endfeet via intercellular signaling. Treating isolated microvessels with IL-6 may mimic neuroinflammatory conditions during which AQP4 is decreased in astrocytic endfeet. A possible route of IL-6 action is the activation of the NF-κB pathway in the wall of microvessels (Sun et al., 2017; Janssens et al., 2015) which

is inhibited by the anti-inflammatory cytokine IL-10 (Driessler et al., 2004). Consequently, IL-10 may antagonize IL-6 effects on AQP4 immunoreactivity pattern, as it was detected in WT microvessels (Figure 14). APOB-100 microvessels, in contrast, did not show a reduction in AQP4 immunoreactive area fraction following IL-6. However, a decrease in AQP4 area fraction was seen after a combined IL-6+IL-10 action. It may indicate that transgenic microvessels are less sensitive to IL-6 than WT microvessels when IL-6 is applied alone. It also suggests that in transgenic microvessels instead of the NF-κB pathway IL-6 and IL-10 may use other signaling pathways, such as the transcription factor STAT3. Both IL-6 and IL-10 can activate STAT3 in brain endothelial cells (Lin et al., 2018; Fasler-Kan et al., 2010), which may explain the lack of antagonism between IL-6 and IL-10 in APOB-100 microvessels.

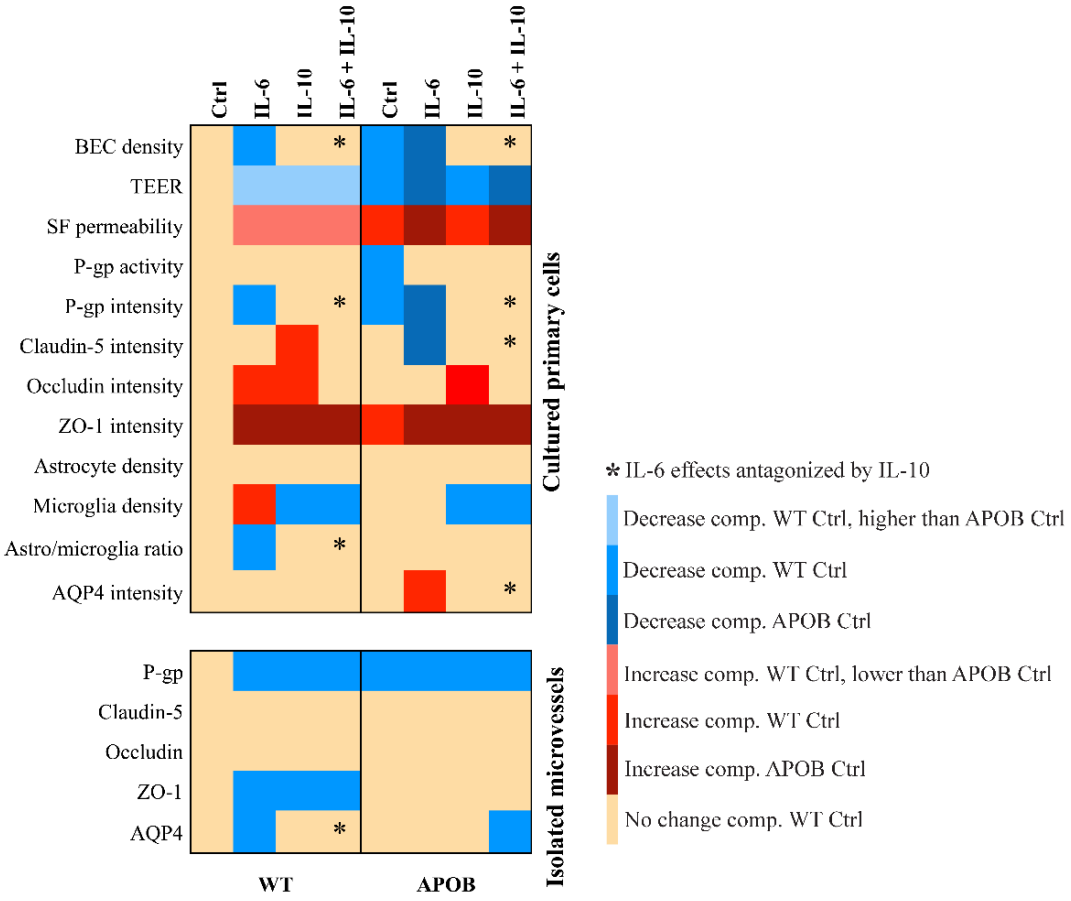

Figure 14. Summary of functional and morphological changes of BBB characteristics in WT and APOB-100 models. Heat map representation of the effects of IL-6 and IL-10 cytokine treatments on BBB characteristics measured in WT and APOB-100 models.

6. Summary

Hypertriglyceridemia is a serious risk factor in the development of cardiovascular diseases and closely linked to atherosclerosis related inflammatory processes, BBB dysfunction and neurodegeneration. Using APOB-100 transgenic mice, an animal model of chronic hypertriglyceridemia, our aim was to study cerebrovascular changes, BBB functions and morphology in APOB-100 transgenic mice *in vivo*, *in vitro* and *ex vivo*. Our objective was to determine which BBB characteristics are produced mainly by IL-6, an atherosclerosis promoting cytokine, and whether these actions can be antagonized by IL-10, an anti-inflammatory cytokine.

We monitored the development of chronic hypertriglyceridemia in 7-, 9- and 12-month-old APOB-100 transgenic animals. We found an increased BBB permeability for SF in the hippocampus of APOB-100 transgenic mice which was accompanied by structural changes. In brain microvessels isolated from APOB-100 transgenic animals an increased *Lox-1* and decreased *Meox-2, Mfsd2a, Abcb1a, Lrp2, Glut-1* gene expressions were measured using quantitative real-time PCR. IL-6 mRNA levels were higher in isolated brain microvessels than in brain parenchyma of APOB-100 transgenic mice. The decreased P-gp/*Abcb1a* gene expression was reflected at protein level too, as demonstrated by immunohistochemical analysis of transgenic brain sections using confocal microscopy, while in the case of occludin and claudin-5 TJ proteins, no changes in immunolabeling pattern was observed.

In our next series of experiments, we demonstrated functional and morphological differences between WT and APOB-100 brain endothelial cells under control conditions. Functional characteristics, such as TEER, SF permeability and P-gp activity were sensitive to both IL-6 and IL-10 cytokine treatments, but no antagonistic effect was observed. In contrast, a decrease in brain endothelial cell density and P-gp immunofluorescence intensity detected in both genotypes following IL-6 treatment was antagonized by IL-10. Other BBB features sensitive to IL-6 in APOB-100 brain endothelial cells included a decrease in claudin-5 and an increase in AQP4 fluorescence intensity, and a decrease in astro-/microglia ratio in WT glia cultures. These IL-6 induced changes were also antagonized by IL-10. Isolated brain microvessels in general, and APOB-100 microvessels in particular, were less reactive to cytokine treatments than cell cultures. In this *ex vivo* system IL-6 resulted in a decrease in P-gp, ZO-1 and AQP4 immunostained area fractions in WT microvessels. The decrease in AQP4 immunolabeled area fraction was antagonized by IL-10. Following treatment with the anti-inflammatory cytokine IL-10 a decrease in P-gp and ZO-1 immunolabeled area fractions

was seen, and no antagonistic effect was observed between IL-6 and IL-10 action regarding P-gp and ZO-1 changes in WT microvessels. Our present results identify BBB characteristics sensitive to either IL-6 or IL-10 actions, and demonstrate for the first time that IL-10 can prevent, at least in part, IL-6 induced BBB impairments.

7. Conclusions

Based on our results we conclude that in chronic hypertriglyceridemic APOB-100 transgenic mice both functional and morphological cerebrovascular pathology can be observed. Therefore, this animal model could be a useful tool to study the link between cerebrovascular damage and neurodegenerative diseases of vascular origin, which is fundamental for the development of efficient therapies.

8. Acknowledgments

I would like to express my gratitude to my supervisors, Prof. Mária Deli and Dr. Zsófia Hoyk, for their support and help they gave during my doctoral studies. The completion of the experiments and preparation of the present dissertation would not have been possible without their guidance.

I am grateful for the kind support and scientific guidance to Dr. Fruzsina Walter from the Biological Barriers Research Group.

I would like to say thank you to Prof. Miklós Sántha, Dr. Melinda Tóth, Dr. Brigitta Dukay from the Institute of Biochemistry, BRC, for their help and collaboration.

I would like to gratefully thank all members of the Biological Barriers Research Group for working together and having their support. I am especially grateful to Dr. András Harazin, Dr. Lilla Barna, Dr. Ana Raquel Santa Maria, Dr. Réka Molnár and Judit Vigh for the long working hours we spent together.

I would like to mention Balázs Hallgas, Eszter Lomen, Éva Kárpáti, members of Navolab Diagnostics team, I owe them with my gratitude to have their support to accomplish my studies.

I would like to thank all the people who helped and supported me during my work, they all contributed to make it happen.

My special thanks and gratitude go for my family and closest friends. They have always had my back.

I acknowledge my gratitude to the Theoretical Medicine Doctoral School for permitting me to participate in their doctoral program and their support.

9. References

Abbott NJ, Patabendige AA, Dolman DE, Yusof SR, Begley DJ. (2010) Structure and function of the blood-brain barrier. Neurobiol Dis. 37(1):13-25.

Al Ahmad A, Taboada CB, Gassmann M, Ogunshola OO. (2011) Astrocytes and pericytes differentially modulate blood-brain barrier characteristics during development and hypoxic insult. J Cereb Blood Flow Metab. 31(2):693-705. doi: 10.1038/jcbfm.2010.148.

Aniszewska A, Chłodzińska N, Bartkowska K, Winnicka MM, Turlejski K, Djavadian RL. (2015) The expression of interleukin-6 and its receptor in various brain regions and their roles in exploratory behavior and stress responses. J Neuroimmunol. 15;284:1-9. doi: 10.1016/j.jneuroim.2015.05.001.

Antonios, N., Angiolillo, D. J., and Silliman, S. (2008) Hypertriglyceridemia and ischemic stroke. Eur. Neurol. 60, 269–278. doi: 10.1159/000157880.

Banks WA, Kovac A, Morofuji Y. (2018) Neurovascular unit crosstalk: Pericytes and astrocytes modify cytokine secretion patterns of brain endothelial cells. J Cereb Blood Flow Metab. 38(6):1104-1118. doi: 10.1177/0271678X17740793.

Bennett J, Basivireddy J, Kollar A, Biron KE, Reickmann P, Jefferies WA, McQuaid S. (2010) Blood-brain barrier disruption and enhanced vascular permeability in the multiple sclerosis model EAE. J Neuroimmunol. 229(1-2):180-91.

Benveniste EN, Whitaker JN, Gibbs DA, Sparacio SM, Butler JL. (1989) Human B cell growth factor enhances proliferation and glial fibrillary acidic protein gene expression in rat astrocytes. Int Immunol. 1989;1(3):219-28. doi: 10.1093/intimm/1.3.219. Erratum in: Int Immunol 1989;1(5):555.

Bereczki E, Bernát G, Csont T, Ferdinandy P, Scheich H, Sántha M. (2008) Overexpression of human apolipoprotein B-100 induces severe neurodegeneration in transgenic mice. J Proteome Res. 7(6):2246 52.

Bjelik A, Bereczki E, Gonda S, Juhász A, Rimanóczy A, Zana M, Csont T, Pákáski M, Boda K, Ferdinandy P, Dux L, Janka Z, Sántha M, Kálmán J (2006) Human apoB overexpression and a high-cholesterol diet differently modify the brain APP metabolism in the transgenic mouse model of atherosclerosis. Neurochem Int 49: 393-400.

Brosseron F, Krauthausen M, Kummer M, Heneka MT. (2014) Body fluid cytokine levels in mild cognitive impairment and Alzheimer's disease: a comparative overview. Mol Neurobiol. 50(2):534-44.

Burgess BL, McIsaac SA, Naus KE, Chan JY, Tansley GHK, Yang J, Miao FD, Ross CJD and others. (2006) Elevated plasma triglyceride levels precede amyloid deposition in Alzheimer's disease mouse models with abundant A beta in plasma. Neurobiol. Dis. 24: 114-127.

Burmeister AR, Marriott I. (2018) The Interleukin-10 Family of Cytokines and Their Role in the CNS. Front Cell Neurosci. 27;12:458. doi: 10.3389/fncel.2018.00458.

Camire RB, Beaulac HJ, Willis CL. (2015) Transitory loss of glia and the subsequent modulation in inflammatory cytokines/chemokines regulate paracellular claudin-5 expression in endothelial cells. J Neuroimmunol. 15;284:57-66. doi: 10.1016/j.jneuroim.2015.05.008.

Campos-Bedolla P, Walter FR, Veszelka S, Deli MA. (2014) Role of the blood-brain barrier in the nutrition of the central nervous system. Arch Med Res. 45(8):610-38.

Chan, L. (1992) Apolipoprotein-B, the major protein component of triglyceride-rich and low-density lipoproteins. J Biol Chem. 267: 25621-25.

Cirrito, J. R., Deane, R., Fagan, A. M., Spinner, M. L., Parsadanian, M., Finn, M. B., et al. (2005) P-glycoprotein deficiency at the blood-brain barrier increases amyloid-beta deposition in an Alzheimer disease mouse model. J. Clin. Invest. 115, 3285–3290. doi: 10.1172/JCI25247.

Cohen SS, Min M, Cummings EE, Chen X, Sadowska GB, Sharma S, Stonestreet BS. (2013) Effects of interleukin-6 on the expression of tight junction proteins in isolated cerebral microvessels from yearling and adult sheep. Neuroimmunomodulation. 2013;20(5):264-73. doi: 10.1159/000350470.

Croop, J. M., Raymond, M., Haber, D., Devault, A., Arceci, R. J., Gros, P., et al. (1989) The three mouse multidrug resistance (mdr) genes are expressed in a tissue-specific manner in normal mouse tissues. Mol. Cell. Biol. 9, 1346–1350. doi: 10.1128/MCB.9.3.1346.

Császár E, Lénárt N, Cserép C, Környei Z, Fekete R, Pósfai B, Balázsfi D, Hangya B, Schwarcz AD, Szabadits E, Szöllősi D, Szigeti K, Máthé D, West BL, Sviatkó K, Brás AR, Mariani JC, Kliewer A, Lenkei Z, Hricisák L, Benyó Z, Baranyi M, Sperlágh B, Menyhárt Á, Farkas E, Dénes Á. (2022) Microglia modulate blood flow, neurovascular coupling, and hypoperfusion via purinergic actions. J Exp Med. 7;219(3):e20211071. doi: 10.1084/jem.20211071.

Csont T, Bereczki E, Bencsik P, Fodor G, Görbe A, Zvara A, Csonka C, Puskás LG, Sántha M, Ferdinandy P. (2007) Hypercholesterolemia increases myocardial oxidative and nitrosative stress thereby leading to cardiac dysfunction in apoB-100 transgenic mice. Cardiovasc Res. 76(1): 100-9.

da Fonseca AC, Matias D, Garcia C, Amaral R, Geraldo LH, Freitas C, Lima FR. (2014) The impact of microglial activation on blood-brain barrier in brain diseases. Front Cell Neurosci. 3;8:362. doi: 10.3389/fncel.2014.00362.

Database of gene expression in adult mouse brain and lung vascular and perivascular cells. http://betsholtzlab.org/VascularSingleCells/database.html. Last accessed 24 Apr 2024.

Deane, R., Du Yan, S., Submamaryan, R. K., LaRue, B., Jovanovic, S., Hogg, E., et al. (2003) RAGE mediates amyloid-beta peptide transport across the blood-brain barrier and accumulation in brain. Nat. Med. 9, 907–113. doi: 10.1038/ nm890.

Decourt B, Lahiri DK, Sabbagh MN. (2017) Targeting Tumor Necrosis Factor Alpha for Alzheimer's Disease. Curr Alzheimer Res. 14(4):412-425.

Deli MA, Abrahám CS, Kataoka Y, Niwa M. (2005) Permeability studies on in vitro blood-brain barrier models: physiology, pathology, and pharmacology. Cell Mol Neurobiol. 25(1):59-127. doi: 10.1007/s10571-004-1377-8.

de Vries HE, Blom-Roosemalen MC, van Oosten M, de Boer AG, van Berkel TJ, Breimer DD, Kuiper J. (1996) The influence of cytokines on the integrity of the blood-brain barrier in vitro. J Neuroimmunol. 64(1):37-43. doi: 10.1016/0165-5728(95)00148-4.

Dinarello CA. (2007) Historical insights into cytokines. Eur J Immunol. 37 Suppl 1(Suppl 1):S34-45. doi: 10.1002/eji.200737772.

Driessler F, Venstrom K, Sabat R, Asadullah K, Schottelius AJ. (2004) Molecular mechanisms of interleukin-10-mediated inhibition of NF-kappaB activity: a role for p50. Clin Exp Immunol. 135(1):64-73. doi: 10.1111/j.1365-2249.2004.02342.x.

Eiselein, L., Wilson, D. W., Lamé, M. W., and Rutledge, J. C. (2007) Lipolysis products from triglyceride-rich lipoproteins increase endothelial permeability, perturb zonula occludens-1 and F-actin, and induce apoptosis. Am. J. Physiol. Heart Circ. Physiol. 292, H2745–H2753. doi: 10.1152/ajpheart.00686. 2006.

Ehrhart J, Smith AJ, Kuzmin-Nichols N, Zesiewicz TA, Jahan I, Shytle RD, Kim SH, Sanberg CD, Vu TH, Gooch CL, Sanberg PR, Garbuzova-Davis S. (2015) Humoral

factors in ALS patients during disease progression. J Neuroinflammation. 28;12:127. doi: 10.1186/s12974-015-0350-4.

Erta M, Quintana A, Hidalgo J. (2012) Interleukin-6, a major cytokine in the central nervous system. Int J Biol Sci. 8(9):1254-66. doi: 10.7150/ijbs.4679.

Farkas G, Márton J, Nagy Z, Mándi Y, Takács T, Deli MA, Abrahám CS. (1998) Experimental acute pancreatitis results in increased blood-brain barrier permeability in the rat: a potential role for tumor necrosis factor and interleukin 6. Neurosci Lett. 20;242(3):147-50. doi: 10.1016/s0304-3940(98)00060-3.

Fasler-Kan E, Suenderhauf C, Barteneva N, Poller B, Gygax D, Huwyler J. (2010) Cytokine signaling in the human brain capillary endothelial cell line hCMEC/D3. Brain Res. 1;1354:15-22. doi: 10.1016/j.brainres.2010.07.077.

Feldmann M, Asselin MC, Liu J, Wang S, McMahon A, Anton-Rodriguez J, Walker M, Symms M, Brown G, Hinz R, Matthews J, Bauer M, Langer O, Thom M, Jones T, Vollmar C, Duncan JS, Sisodiya SM, Koepp MJ. (2013) P-glycoprotein expression and function in patients with temporal lobe epilepsy: a case-control study. Lancet Neurol. 12(8):777-85. doi: 10.1016/S1474-4422(13)70109-1.

Fernandez C, Buyse M, German-Fattal M, Gimenez F. (2004) Influence of the pro-inflammatory cytokines on P-glycoprotein expression and functionality. J Pharm Pharm Sci. 17;7(3):359-71.

Fletcher SJ, Iqbal M, Jabbari S, Stekel D, Rappoport JZ. (2014) Analysis of occludin trafficking, demonstrating continuous endocytosis, degradation, recycling and biosynthetic secretory trafficking. PLoS One. 25;9(11):e111176. doi: 10.1371/journal.pone.0111176.

Glass CK, Witztum JL. (2001) Atherosclerosis. the road ahead. Cell. 23;104(4):503-16. doi: 10.1016/s0092-8674(01)00238-0.

Greenwood J. (1992) Characterization of a rat retinal endothelial cell culture and the expression of P-glycoprotein in brain and retinal endothelium in vitro. J Neuroimmunol. 39(1-2):123-32. doi: 10.1016/0165-5728(92)90181-j.

Günzel D, Yu AS. (2013) Claudins and the modulation of tight junction permeability. Physiol Rev. 93(2):525-69. doi: 10.1152/physrev.00019.2012.

Hartz AM, Bauer B, Fricker G, Miller DS. (2006) Rapid modulation of P-glycoprotein-mediated transport at the blood-brain barrier by tumor necrosis factor-alpha and lipopolysaccharide. Mol Pharmacol. 69(2):462-70. doi: 10.1124/mol.105.017954.

He L, Vanlandewijck M, Mäe MA, Andrae J, Ando K, Del Gaudio F, Nahar K, Lebouvier T, Laviña B, Gouveia L, Sun Y, Raschperger E, Segerstolpe Å, Liu J, Gustafsson S, Räsänen M, Zarb Y, Mochizuki N, Keller A, Lendahl U, Betsholtz C. (2018) Single-cell RNA sequencing of mouse brain and lung vascular and vessel-associated cell types. Sci Data. 21;5:180160. doi: 10.1038/sdata.2018.160.

Hellinger E, Veszelka S, Tóth AE, Walter F, Kittel A, Bakk ML, Tihanyi K, Háda V, Nakagawa S, Duy TD, Niwa M, Deli MA, Vastag M. (2012) Comparison of brain capillary endothelial cell-based and epithelial (MDCK-MDR1, Caco-2, and VB-Caco-2) cell-based surrogate blood-brain barrier penetration models. Eur J Pharm Biopharm. 82(2):340-51. doi: 10.1016/j.ejpb.2012.07.020.

Helms HC, Hersom M, Kuhlmann LB, Badolo L, Nielsen CU, Brodin B. (2014) An electrically tight in vitro blood-brain barrier model displays net brain-to-blood efflux of substrates for the ABC transporters, P-gp, Bcrp and Mrp-1. AAPS J. 16(5):1046-55. doi: 10.1208/s12248-014-9628-1.

Hersh J, Prah J, Winters A, Liu R, Yang SH. (2021) Modulation of astrocyte phenotype in response to T-cell interaction. J Neuroimmunol. 15;351:577455. doi: 10.1016/j.jneuroim.2020.577455.

Hoyk Z, Tóth ME, Lénárt N, Nagy D, Dukay B, Csefová A, Zvara Á, Seprényi G, Kincses A, Walter FR, Veszelka S, Vígh J, Barabási B, Harazin A, Kittel Á, Puskás LG, Penke B, Vígh L, Deli MA, Sántha M. (2018) Cerebrovascular Pathology in Hypertriglyceridemic APOB-100 Transgenic Mice. Front Cell Neurosci. 25;12:380. doi: 10.3389/fncel.2018.00380.

Hubbard JA, Szu JI, Binder DK. (2018) The role of aquaporin-4 in synaptic plasticity, memory and disease. Brain Res Bull. 136:118-129. doi: 10.1016/j.brainresbull.2017.02.011.

Iqbal M, Ho HL, Petropoulos S, Moisiadis VG, Gibb W, Matthews SG. (2012) Pro-inflammatory cytokine regulation of P-glycoprotein in the developing blood-brain barrier. PLoS One. 7(8):e43022. doi: 10.1371/journal.pone.0043022.

Janssens K, Slaets H, Hellings N. (2015) Immunomodulatory properties of the IL-6 cytokine family in multiple sclerosis. Ann N Y Acad Sci. 1351:52-60. doi: 10.1111/nyas.12821.

Jonkers IJ, Mohrschladt MF, Westendorp RG, van der Laarse A, Smelt AH. (2002) Severe hypertriglyceridemia with insulin resistance is associated with systemic inflammation: reversal with bezafibrate therapy in a randomized controlled trial. Am J Med. 112(4):275-80. doi: 10.1016/s0002-9343(01)01123-8.

Kishikawa H, Shimokama T, Watanabe T. (1993) Localization of T lymphocytes and macrophages expressing IL-1, IL-2 receptor, IL-6 and TNF in human aortic intima. Role of cell-mediated immunity in human atherogenesis. Virchows Arch A Pathol Anat Histopathol. 423(6):433-42. doi: 10.1007/BF01606532.

Kloss CU, Kreutzberg GW, Raivich G. (1997) Proliferation of ramified microglia on an astrocyte monolayer: characterization of stimulatory and inhibitory cytokines. J Neurosci Res. 15;49(2):248-54. doi: 10.1002/(SICI) 1097-4547(19970715)49:2%3c248::AID-JNR13%3e3.0.CO;2-X.

Koenigsknecht-Talboo J, Landreth GE. (2005) Microglial phagocytosis induced by fibrillar beta-amyloid and IgGs are differentially regulated by proinflammatory cytokines. J Neurosci. 25(36):8240-9.

Kovac A, Erickson MA, Banks WA. (2011) Brain microvascular pericytes are immunoactive in culture: cytokine, chemokine, nitric oxide, and LRP-1 expression in response to lipopolysaccharide. J Neuroinflammation. 13;8:139. doi: 10.1186/1742-2094-8-139.

Lee, L. L., Aung, H. H., Wilson, D. W., Anderson, S. E., Rutledge, J. C., and Rutkowsky, J. M. (2017) Triglyceride-rich lipoprotein lipolysis products increase blood-brain barrier transfer coefficient and induce astrocyte lipid droplets and cell stress. Am. J. Physiol. Cell Physiol. 312, C500–C516. doi: 10.1152/ajpcell.00120.2016.

Ledeboer A, Brevé JJ, Wierinckx A, van der Jagt S, Bristow AF, Leysen JE, Tilders FJ, Van Dam AM. (2002) Expression and regulation of interleukin-10 and interleukin-10 receptor in rat astroglial and microglial cells. Eur J Neurosci. 16(7):1175-85. doi: 10.1046/j.1460-9568.2002.02200.x.

Lénárt N, Szegedi V, Juhász G, Kasztner A, Horváth J, Bereczki E, Tóth ME, Penke B, Sántha M. (2012) Increased tau phosphorylation and impaired presynaptic function in hypertriglyceridemic ApoB-100 transgenic mice. PlosOne.; 7(9): e46007.

Lénárt N, Walter FR, Bocsik A, Sántha P, Tóth ME, Harazin A, Tóth AE, Vizler C, Török Z, Pilbat AM, Vígh L, Puskás LG, Sántha M, Deli MA. (2015) Cultured cells of the blood-brain barrier from apolipoprotein B-100 transgenic mice: effects of oxidized low-density lipoprotein treatment. Fluids Barriers CNS. 12:17.

Lin R, Chen F, Wen S, Teng T, Pan Y, Huang H. (2018) Interleukin-10 attenuates impairment of the blood-brain barrier in a severe acute pancreatitis rat model. J Inflamm (Lond). 27;15:4. doi: 10.1186/s12950-018-0180-0.

Lobo-Silva, D., Carriche, G.M., Castro, A.G. et al. (2016) Balancing the immune response in the brain: IL-10 and its regulation. J Neuroinflammation **13**, 297. https://doi.org/10.1186/s12974-016-0763-8

Löffler T, Flunkert S, Havas D, Sántha M, Hutter-Paier B, Steyrer E, Windisch M. (2013) Impact of ApoB-100 expression on cognition and brain pathology in wild-type and hAPPsl mice. Neurobiol Aging. 34(10):2379-88.

Lucero D, Islam P, Freeman LA, Jin X, Pryor M, Tang J, Kruth HS, Remaley AT. (2020) Interleukin 10 promotes macrophage uptake of HDL and LDL by stimulating fluid-phase endocytosis. Biochim Biophys Acta Mol Cell Biol Lipids. 1865(2):158537. doi: 10.1016/j.bbalip.2019.158537.

Martins IJ, Berger T, Sharman MJ, Verdile G, Fuller SJ, et al. (2009) Cholesterol metabolism and transport in the pathogenesis of Alzheimer's disease. J Neurochem 111:1275–1308.

Mathiisen TM, Lehre KP, Danbolt NC, Ottersen OP. (2010) The perivascular astroglial sheath provides a complete covering of the brain microvessels: an electron microscopic 3D reconstruction. Glia. 58(9):1094-103. doi: 10.1002/glia.20990.

Mohamed LA, Markandaiah S, Bonanno S, Pasinelli P, Trotti D. (2017) Blood-Brain Barrier Driven Pharmacoresistance in Amyotrophic Lateral Sclerosis and Challenges for Effective Drug Therapies. AAPS J. 19(6):1600-1614. doi: 10.1208/s12248-017-0120-6.

Murray PJ. (2005) The primary mechanism of the IL-10-regulated antiinflammatory response is to selectively inhibit transcription. Proc Natl Acad Sci U S A. 14;102(24):8686-91. doi: 10.1073/pnas.0500419102.

Nakagawa S, Deli MA, Kawaguchi H, Shimizudani T, Shimono T, Kittel A, Tanaka K, Niwa M. (2009) A new blood-brain barrier model using primary rat brain endothelial cells, pericytes and astrocytes. Neurochem Int. 54(3-4):253-63. doi: 10.1016/j.neuint.2008.12.002.

Ono S, Hu J, Shimizu N, Imai T, Nakagawa H. (2001) Increased interleukin-6 of skin and serum in amyotrophic lateral sclerosis. J Neurol Sci. 15;187(1-2):27-34. doi: 10.1016/s0022-510x(01)00514-7.

Otsu, N. (1979) A Threshold Selection Method from Gray-Level Histograms. IEEE Transactions on Systems, Man, and Cybernetics, vol. 9, no. 1, pp. 62-66, doi: 10.1109/TSMC.1979.4310076.

Patterson, C. E., Rhoades, R. A., and Garcia, J. G. (1992) Evans blue dye as a marker of albumin clearance in cultured endothelial monolayer and isolated lung. J. Appl. Physiol. 72, 865–873. doi: 10.1152/jappl.1992.72. 3.865.

Perrière N, Demeuse P, Garcia E, Regina A, Debray M, et al. (2005) Puromycin-based purification of rat brain capillary endothelial cell cultures. Effect on the expression of blood-brain barrier-specific properties. J Neurochem. 2005;93:279-289.

Petković F, Castellano B. (2016) The role of interleukin-6 in central nervous system demyelination. Neural Regen Res. 11(12):1922-1923.

Poller B, Drewe J, Krähenbühl S, Huwyler J, Gutmann H. (2010) Regulation of BCRP (ABCG2) and P-glycoprotein (ABCB1) by cytokines in a model of the human blood-brain barrier. Cell Mol Neurobiol. 30(1):63-70. doi: 10.1007/s10571-009-9431-1.

Ramirez SH, Fan S, Dykstra H, Rom S, Mercer A, Reichenbach NL, Gofman L, Persidsky Y. (2013) Inhibition of glycogen synthase kinase 3β promotes tight junction stability in brain endothelial cells by half-life extension of occludin and claudin-5. PLoS One. 8(2):e55972. doi: 10.1371/journal.pone.0055972.

Recasens M, Shrivastava K, Almolda B, González B, Castellano B. (2019) Astrocyte-targeted IL-10 production decreases proliferation and induces a downregulation of

activated microglia/macrophages after PPT. Glia. 67(4):741-758. doi: 10.1002/glia.23573.

Recasens M, Almolda B, Pérez-Clausell J, Campbell IL, González B, Castellano B. (2021) Chronic exposure to IL-6 induces a desensitized phenotype of the microglia. J Neuroinflammation. 22;18(1):31. doi: 10.1186/s12974-020-02063-1.

Ridker PM. (2016) From C-Reactive Protein to Interleukin-6 to Interleukin-1: Moving Upstream To Identify Novel Targets for Atheroprotection. Circ Res. 8;118(1):145-56. doi: 10.1161/CIRCRESAHA.115.306656.

Rochfort KD, Collins LE, Murphy RP, Cummins PM. (2014) Downregulation of blood-brain barrier phenotype by proinflammatory cytokines involves NADPH oxidase-dependent ROS generation: consequences for interendothelial adherens and tight junctions. PLoS One. 3;9(7):e101815. doi: 10.1371/journal.pone.0101815.

Rochfort KD, Cummins PM. (2015) Cytokine-mediated dysregulation of zonula occludens-1 properties in human brain microvascular endothelium. Microvasc Res. 100:48-53. doi: 10.1016/j.mvr.2015.04.010.

Ross R, Harker L. (1976) Hyperlipidemia and atherosclerosis. Science. 17;193(4258):1094-100. doi: 10.1126/science.822515.

Rubio-Perez JM, Morillas-Ruiz JM. (2012) A review: inflammatory process in Alzheimer's disease, role of cytokines. ScientificWorldJournal. 2012:756357.

Sasson E, Anzi S, Bell B, Yakovian O, Zorsky M, Deutsch U, Engelhardt B, Sherman E, Vatine G, Dzikowski R, Ben-Zvi A. (2021) Nano-scale architecture of blood-brain barrier tight-junctions. Elife. 24;10:e63253. doi: 10.7554/eLife.63253.

Schwenke DC, Carew TE. (1989) Initiation of atherosclerotic lesions in cholesterol-fed rabbits. II. Selective retention of LDL vs. selective increases in LDL permeability in susceptible sites of arteries. Arteriosclerosis. 9(6):908-18. doi: 10.1161/01.atv.9.6.908.

Schissel SL, Jiang X, Tweedie-Hardman J, Jeong T, Camejo EH, Najib J, Rapp JH, Williams KJ, Tabas I. (1998) Secretory sphingomyelinase, a product of the acid sphingomyelinase gene, can hydrolyze atherogenic lipoproteins at neutral pH. Implications for atherosclerotic lesion development. J Biol Chem. 30;273(5):2738-46. doi: 10.1074/jbc.273.5.2738.

Selmaj KW, Farooq M, Norton WT, Raine CS, Brosnan CF. (1990) Proliferation of astrocytes in vitro in response to cytokines. A primary role for tumor necrosis factor. J Immunol. 1;144(1):129-35.

Segrest JP, Jones MK, De Loof H, Dashti N. (2001) Structure of apolipoprotein B-100 in low density lipoproteins J Lipid Res. 42:1346-67.

Seino Y, Ikeda U, Ikeda M, Yamamoto K, Misawa Y, Hasegawa T, Kano S, Shimada K. (1994) Interleukin 6 gene transcripts are expressed in human atherosclerotic lesions. Cytokine. 6(1):87-91. doi: 10.1016/1043-4666(94)90013-2.

Shibata, M., Yamada, S., Kumar, S. R., Calero, M., Bading, J., Frangione, B., et al. (2000) Clearance of Alzheimer’s amyloid-beta (1-40) peptide from brain by LDL receptor-related protein-1 at the blood-brain barrier. J. Clin. Invest. 106, 1489–1499. doi: 10.1172/JCI10498.

Shoshani, T., Zhang, S., Dey, S., Pastan, I., and Gottesman, M. M. (1998) Analysis of random recombination between human MDR1 and mouse mdr1a cDNA in a pHaMDR-dihydrofolate reductase bicistronic expression system. Mol. Pharmacol. 54, 623–630.

Sugimoto N, Leu H, Inoue N, Shimizu M, Toma T, Kuroda M, Saito T, Wada T, Yachie A. (2015) The critical role of lipopolysaccharide in the upregulation of aquaporin 4 in glial cells treated with Shiga toxin. J Biomed Sci. 18;22(1):78. doi: 10.1186/s12929-015-0184-5.

Sukhai M, Yong A, Pak A, Piquette-Miller M. (2001) Decreased expression of P-glycoprotein in interleukin-1beta and interleukin-6 treated rat hepatocytes. Inflamm Res. 50(7):362-70. doi: 10.1007/PL00000257.

Sun L, Li M, Ma X, Feng H, Song J, Lv C, He Y. (2017) Inhibition of HMGB1 reduces rat spinal cord astrocytic swelling and AQP4 expression after oxygen-glucose deprivation and reoxygenation via TLR4 and NF-κB signaling in an IL-6-dependent manner. J Neuroinflammation. 25;14(1):231. doi: 10.1186/s12974-017-1008-1.

Süle, Z., Mracskó, E., Bereczki, E., Sántha, M., Csont, T., Ferdinandy, P., et al. (2009) Capillary injury in the ischemic brain of hyperlipidemic, apolipoprotein B-100 transgenic mice. Life Sci. 84, 935–939. doi: 10.1016/j.lfs.2009.04.011.

Streit WJ, Hurley SD, McGraw TS, Semple-Rowland SL. (2000) Comparative evaluation of cytokine profiles and reactive gliosis supports a critical role for interleukin-6 in neuron-glia signaling during regeneration. J Neurosci Res. 1;61(1):10-20. doi: 10.1002/1097-4547(20000701)61:1<10::AID-JNR2>3.0.CO;2-E.

Sweeney MD, Sagare AP, Zlokovic BV. (2018) Blood-brain barrier breakdown in Alzheimer disease and other neurodegenerative disorders. Nat Rev Neurol. 14:133-150.

Szczepkowska A, Harazin A, Barna L, Deli MA, Skipor J. (2021) Identification of Reference Genes for Circadian Studies on Brain Microvessels and Choroid Plexus Samples Isolated from Rats. Biomolecules. 17;11(8):1227. doi: 10.3390/biom11081227.

Tedgui A, Mallat Z. (2006) Cytokines in atherosclerosis: pathogenic and regulatory pathways. Physiol Rev. 86(2):515-81. doi: 10.1152/physrev.00024.2005.

Tornavaca O, Chia M, Dufton N, Almagro LO, Conway DE, Randi AM, Schwartz MA, Matter K, Balda MS. (2015) ZO-1 controls endothelial adherens junctions, cell-cell tension, angiogenesis, and barrier formation. J Cell Biol. 16;208(6):821-38. doi: 10.1083/jcb.201404140.

Tóth ME, Dukay B, Hoyk Z, Sántha M. (2020) Cerebrovascular Changes and Neurodegeneration Related to Hyperlipidemia: Characteristics of the Human ApoB-100 Transgenic Mice. Curr Pharm Des. 26(13):1486-1494. doi: 10.2174/1381612826666200218101818.

Vanlandewijck M, He L, Mäe MA, Andrae J, Ando K, Del Gaudio F, Nahar K, Lebouvier T, Laviña B, Gouveia L, Sun Y, Raschperger E, Räsänen M, Zarb Y, Mochizuki N, Keller A, Lendahl U, Betsholtz C. (2018) A molecular atlas of cell types and zonation in the brain vasculature. Nature. 22;554(7693):475-480. doi: 10.1038/nature25739.

Verma S, Nakaoke R, Dohgu S, Banks WA. (2006) Release of cytokines by brain endothelial cells: A polarized response to lipopolysaccharide. Brain Behav Immun. 20(5):449-55. doi: 10.1016/j.bbi.2005.10.005.

Veszelka, S., Urbányi, Z., Pázmány, T., Németh, L., Obál, I., Dung, N. T., et al. (2003) Human serum amyloid P component attenuates the bacterial lipopolysaccharide-induced increase in blood-brain barrier permeability in mice. Neurosci. Lett. 352, 57–60. doi: 10.1016/j.neulet.2003.08.028.

Veszelka S, Pásztói M, Farkas AE, Krizbai I, Ngo TK, Niwa M, Abrahám CS, Deli MA. (2007) Pentosan polysulfate protects brain endothelial cells against bacterial lipopolysaccharide-induced damages. Neurochem Int. 50(1):219-28. doi: 10.1016/j.neuint.2006.08.006.

Walter FR, Harazin A, Tóth AE, Veszelka S, Santa-Maria AR, Barna L, Kincses A, Biczó G, Balla Z, Kui B, Maléth J, Cervenak L, Tubak V, Kittel Á, Rakonczay Z Jr, Deli MA. (2022) Blood-brain barrier dysfunction in L-ornithine induced acute pancreatitis in rats and the direct effect of L-ornithine on cultured brain endothelial cells. Fluids Barriers CNS. 17;19(1):16. doi: 10.1186/s12987-022-00308-0.

Wigmore SJ, Sangster K, McNally SJ, Harrison EM, Ross JA, Fearon KC, Garden OJ. (2007) De-repression of heat shock transcription factor-1 in interleukin-6-treated hepatocytes is mediated by downregulation of glycogen synthase kinase 3beta and MAPK/ERK-1. Int J Mol Med. 19(3):413-20. doi: 10.3892/ijmm.19.3.413.

Winkler, E. A., Nishida, Y., Sagare, A. P., Rege, S. V., Bell, R. D., Perlmutter, D., et al. (2015) GLUT1 reductions exacerbate Alzheimer's disease vasculo-neuronal dysfunction and degeneration. Nat. Neurosci. 18, 521–530. doi: 10.1038/nn.

Wolburg-Buchholz K, Mack AF, Steiner E, Pfeiffer F, Engelhardt B, Wolburg H. (2009) Loss of astrocyte polarity marks blood-brain barrier impairment during experimental autoimmune encephalomyelitis. Acta Neuropathol. 118(2):219-33. doi: 10.1007/s00401-009-0558-4.

Wolburg H, Noell S, Mack A, Wolburg-Buchholz K, Fallier-Becker P. (2009) Brain endothelial cells and the glio-vascular complex. Cell Tissue Res. 335(1):75-96. doi: 10.1007/s00441-008-0658-9.

Yang J, Lunde LK, Nuntagij P, Oguchi T, Camassa LM, Nilsson LN, Lannfelt L, Xu Y, Amiry-Moghaddam M, Ottersen OP, Torp R. (2011) Loss of astrocyte polarization in the tg-ArcSwe mouse model of Alzheimer's disease. J Alzheimers Dis. 2011;27(4):711-22. doi: 10.3233/JAD-2011-110725.

Zhao Z, Nelson AR, Betsholtz C, Zlokovic BV. (2015) Establishment and Dysfunction of the Blood-Brain Barrier. Cell. 163:1064–78. https://doi.org/10. 1016/j.cell.2015.10.067.

Zlokovic BV. (2011) Neurovascular pathways to neurodegeneration in Alzheimer's disease and other disorders. Nat Rev Neurosci. 12(12):723-38.